CHAPTER 6

# Structural Analysis of Propellant Grains

BERNARD GONDOUIN

## 1. Introduction

Causes of operational failures of solid rocket motors are varied, but the major causes are tied to the structural integrity of the propellants. During their entire service life propellants are subjected to stresses which, in some cases, cause cracks in the propellant grain or separation between the propellant and the inhibitor or the liner. During firing, there are a large number of possible consequences from one of these structural failures.

### 1.1. PROPELLANT STRUCTURAL FAILURE

A crack in the propellant grain results in additional burning surface. The increase in pressure resulting from this accidental increase of the burning surface may lead to either the destruction of the motor, if the pressure is greater than the burst pressure of the motor case, or operation outside of the specifications (modification of the thrust, the burning time, etc.).

### 1.2. BONDING SEPARATION

A bondline separation, when it results in an increase of the burning surface, triggers the same occurrences as described above. Another type of failure may occur, however. The bonding of the propellant with the other materials (inhibitor or thermal protection) is usually located somewhere close to the wall of the case; burning in the debonded area may cause a significant heating for the structure with a risk of burnthrough that would result in an abnormal, and possibly catastrophic, operation of the rocket motor.

There are two very distinct stages in the operational life of a propellant grain:

- the stage before firing: this includes manufacturing followed by various transportation and storage phases. The duration of this stage varies, and could last from a few months to several years.
- the firing, which lasts from a few milliseconds to several seconds, depending on the function expected from the motor.

The mechanical design problem that needs to be solved is the assessment of the risk of a structural failure occurring in the propellant grain and that of debonding during the two stages mentioned above.

An initial method of handling this problem would consist in taking a number of samples during the manufacture of the propellant grains and performing a variety of tests under well-defined conditions. This experimental method requires a large number of tests. It can be contemplated for small objects, with short and easy-to-implement operational conditions. In the case of propellant grains for rocket motors, where dimensions can be quite large and operational conditions difficult to reproduce, a large number of tests are not feasible.

An analytical method allowing the determination, *a priori*, of the structural integrity of the propellant grains seems better indicated. The principle is simple, and consists of determining two values for each loading condition (corresponding to the various phases of the service life). These values are the induced stress or strain resulting from induced loads in the propellant grains, and the allowable stress or strain.

In general, the induced stress or strain in a propellant grain is the maximum stress or strain developed in the propellant. It is found at the location where the propellant is the most mechanically constrained, known as the "critical point." The assumption is as follows: the level of stress/strain at points surrounding the critical point does not influence the structural failure risk of the propellant.

The location of the critical point and corresponding stress and strain are generally determined using a numerical method (finite element method).

The "capability" or allowable stress or strain is the structural stress or strain that must be induced in a propellant grain to cause a structural failure. This value is determined through tests; it is a function of the stress and/or strain measured at the point of structural failure of the test specimens during the various mechanical properties tests performed on the propellant.

The ratio of the capability versus the load gives the factor of safety:

$$K = \frac{C}{S} \quad \text{with} \quad \begin{array}{l} K > 1 \text{ no structural failure} \\ K < 1 \text{ structural failure} \end{array}$$

where:

$C$ = capability of the propellant;
$S$ = induced stress or strain in propellant grain.



If $C$ and $S$ have exact values, this factor must always be greater than 1 to ensure proper mechanical performance of the rocket motor. The variable nature of physical phenomena involved requires a probabilistic approach. The probability of the capability being greater than the induced stress/strain is assessed: it is the structural reliability $F$:

$$F = Pb(K > 1) = Pb(C > S)$$

The analytical method used for this purpose is discussed in this chapter. An overview is provided in Fig. 1. The following questions will be addressed:

- description of the mechanical loads found in propellant grains;
- mechanical properties of the bonding;
- determination of the stress/strain in propellant grains;
- determination of the grain structural integrity.

*Note*: When assessing the grain structural integrity, another value is sometimes determined: the margin of safety, MS. It is written as follows:

$$\text{MS} = \frac{C - S}{S} = K - 1$$

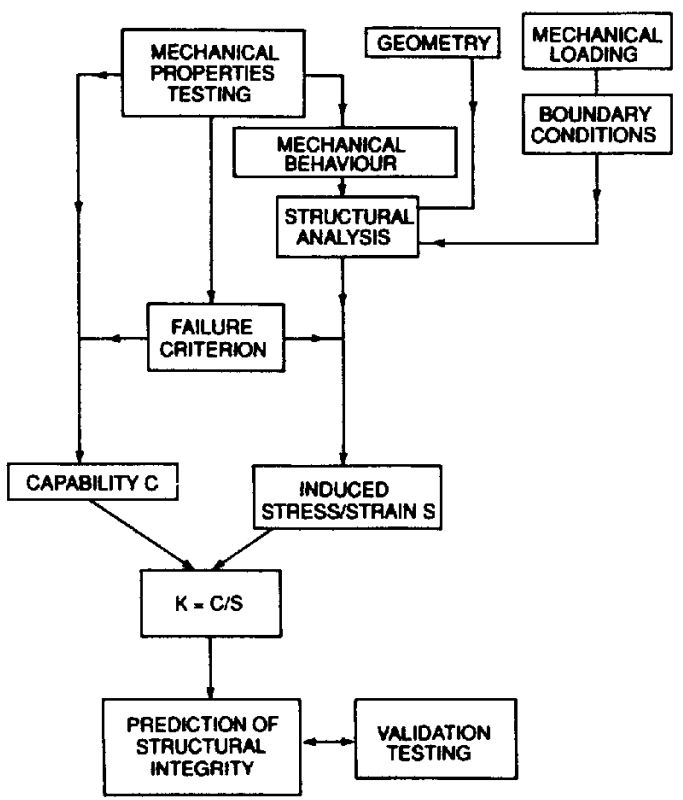


FIG. 6.1. Determination of the structural integrity.

Therefore, the reliability is the probability that the margin of safety is greater than zero:

$$F = Pb(\mathrm{MS} > 0)$$

## 2. Description of the Mechanical Loads

The service life of a propellant grain before firing consists of a succession of transport and storage phases, under conditions that are contingent upon the mission of the missile.

The transport of a space missile to the launching site, for example, happens only once. The propellant is subject to low magnitudes of vibrations, and the temperature variations are often controlled.

Repeated transports of tactical missiles stored or carried beneath an aircraft subject the propellant grain to major accelerations, vibration, and temperature variations. Furthermore, storage of all rocket motors causes creeping due to the effect of the gravity; and because of repeated and various handling, the risks of falls or shocks are certainly not negligible. Lastly, at the time of firing, the pressure rise in the combustion chamber and the acceleration resulting from the induced thrust impose loads on the propellant grain, in addition to those already induced during the pre-firing phase.

To analyze the effect of these various environments on the stress/strain imposed on the propellant, it is necessary to make a distinction between the two major families of propellant grains:

- case-bonded grains;
- free-standing or cartridge-loaded grains.

### 2.1. CASE BONDED GRAINS

#### *2.1.1. Temperature changes*

At the time of its manufacture the propellant grain is cast in the insulated case. The propellant hardens and bonds with the case or its thermal protection with the help of a liner at a temperature which is typically greater than 40°C, known as the cure temperature. Following the curing phase the propellant, subjected to temperatures that are lower than the curing temperature, induces a change in its volume. This change is bound to induce stress/strain in the propellant because it is bonded to a rigid structure with a lower thermal expansion coefficient. A field of thermal stress occurs. The sketches in Fig. 2 illustrate this phenomenon on a cylindrical propellant grain.

In addition to the thermal stresses caused by temperature changes evenly throughout the propellant grain, there are the stresses from thermal gradients occurring during transient phases. These stresses play a greater role in the propellant grain contained in tactical missile motors, where the temperature changes are sometimes very quick.



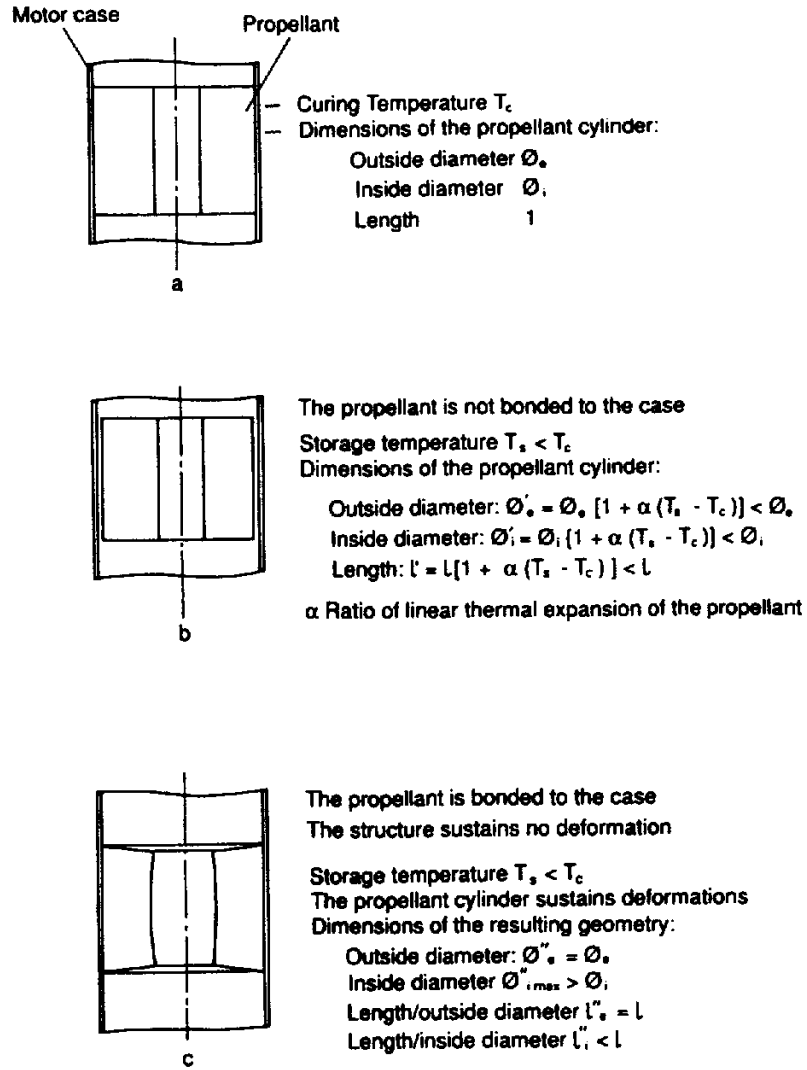


FIG. 6.2. Diagram of the effect of thermal shrinkage.

#### *2.1.2. Force of gravity*

Long-term storage of a case-bonded propellant grain brings on a creeping of the propellant grain due to the force of gravity. The motor case is usually sufficiently rigid to keep its original shape. The strains observed on a cylindrical case-bonded grain due to the effect of gravity are illustrated in Fig. 3.

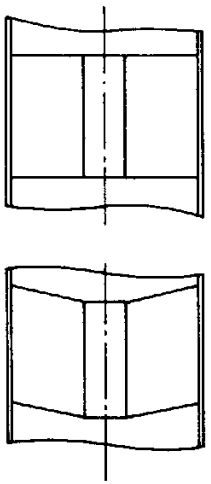


FIG. 6.3. Diagram of the effects of gravity.

### 2.1.3. *Pressure rise at firing*

When a case-bonded propellant grain is fired, the pressure in the combustion chamber increases within a few milliseconds to reach maximum operating pressure. Through the entire time the pressure is transmitted through the propellant to the motor case. The deformation of the case induces a strain field in the propellant and stresses at the bondline.

The strains occurring in a cylindrical propellant grain at the time of pressure rise in the combustion chamber are shown in Fig. 4.

The combustion chamber pressure, at the time of firing, is not steady. There may be significant variations, resulting in a deformation of the combustion chamber, and as result all of the propellant grain faces are subjected to different pressures.

Finally, eventual combustion instabilities may trigger a vibration state in the propellant grain.

### 2.1.4. *Curing under pressure*

In Section 2.1.1 the effects of temperature changes on a case-bonded grain are described. In a case where, during its entire service life, a motor is stored after curing under controlled temperature conditions, the only thermal loads intervening are due to the difference between curing and storage temperatures. If it were possible to compensate for the variation in geometry due to the thermal shrinkage with an equivalent change of geometry, the thermally induced strain would decrease: it is the principle of curing under pressure. A cylindrical case-bonded grain cured under pressure is described in Fig. 5.



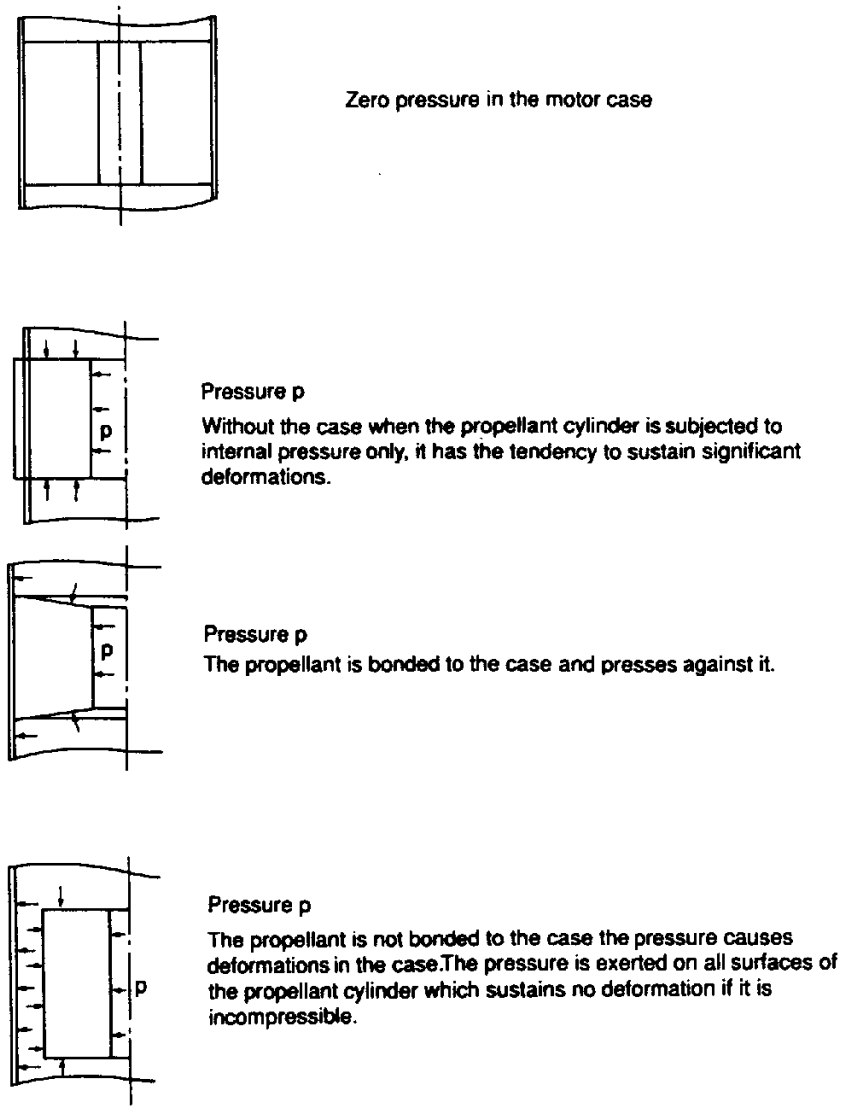


FIG. 6.4. Diagram of the pressure rise induced by firing.

Because in modern motor cases the deformations are small in the cylindrical part, the pressures that should be induced to compensate completely for the thermal shrinkage would simply be too great. Nevertheless, even a partial compensation for the thermal shrinkage permits a reduction of the stresses along the bondline and a decrease in the damage to the propellant grain before its firing.

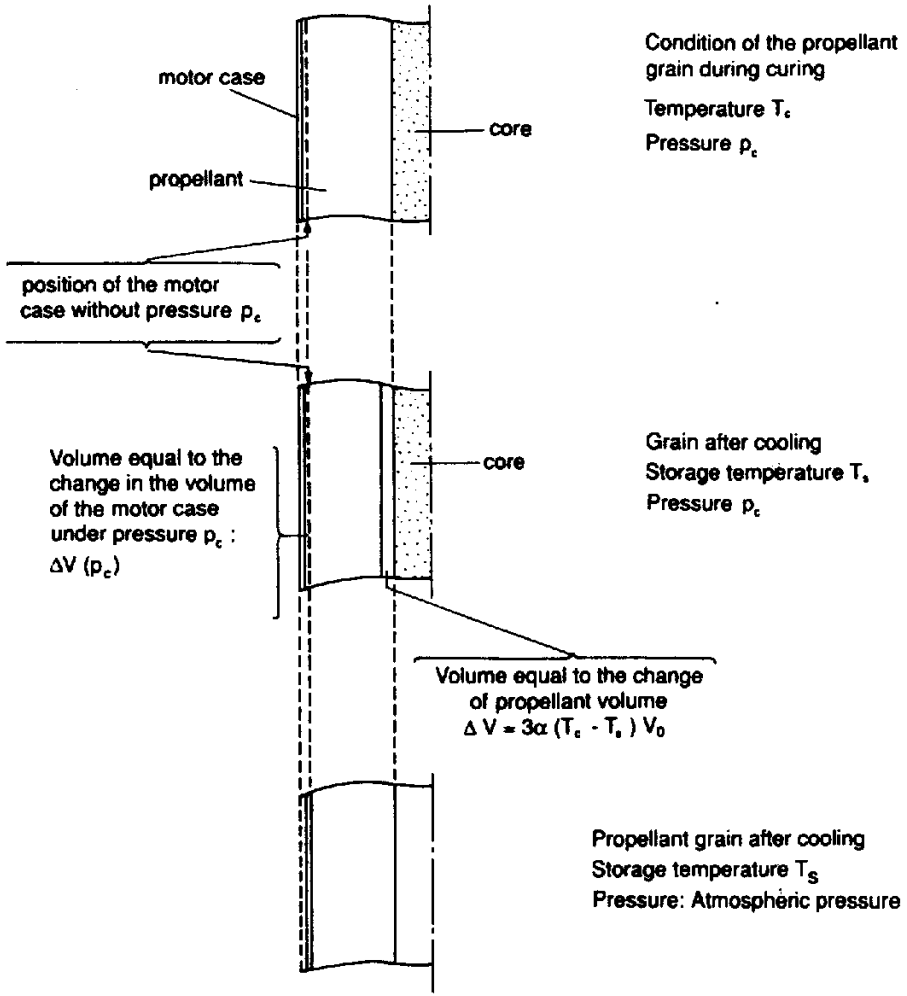


FIG. 6.5. Diagram of the principle of curing under pressure.

## 2.2. FREE-STANDING GRAINS

The major differences between the mechanical loads induced in case-bonded grains and free-standing grains occur during propellant temperature changes and pressure rises at firing. Theoretically there should not be any stress/strain in a free-standing grain under thermal and pressurization loads. (Figs 2b and 4d). In fact, there are transient phases for these two types of loading conditions that eventually could create significant stress/strain.



### 2.2.1. *Temperature changes*

When a change in temperature occurs that is even throughout the propellant grain, a free-standing grain deforms freely, and no strain results. This is the case illustrated in Fig. 2b.

In transient phases, during which the temperature is different in each point of the propellant grain, thermal stress/strain is created. In any type of thermal cycle these thermal stresses are non-existent at the initial and final stabilized temperatures; they can be measured only during the cycle (Fig. 6).

The maximum stress/strain value of a cycle depends on the distribution of the temperatures in the propellant. Consequently, this particular stress/strain is a function of the thermal properties of the material (thermal conductivity of the propellant), of the boundary thermal conditions (convective heat transfer, radiating heat transfer), and of the geometry of the propellant grain.

### 2.2.2. *Pressure rise at firing*

In the steady phase at firing, if the pressure is applied on all faces of the propellant, the resulting stresses/strains are those occurring when a motor case is subjected to an even pressure: it is known as an isostatic state of the stress/strain.

During the unsteady phase the pressure in the combustion chamber and the pressure taking place in the gaps between the propellant grain and the case may increase at a different rate. The grain is thus subjected to pressure gradients causing stress/strain in the propellant. At least two different possibilities have been observed.

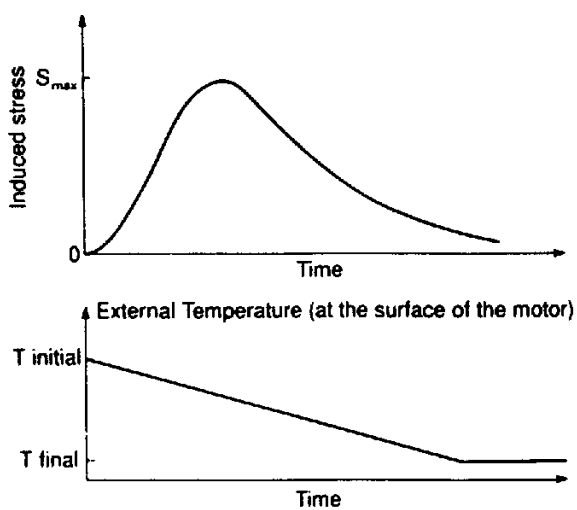


FIG. 6.6. Effects of a temperature change in a free-standing grain.

(a) *Regular pressure increase in the gaps*

The maximum pressure gradient to which the propellant grain is subjected depends on the manner in which the pressure increases in the gap. Figure 7 illustrates the pressure evolutions for a cylindrical propellant grain with a central port.

The question then consists in determining whether the propellant grain can withstand the evolution of the pressure difference $\Delta p(t)$.

(b) *Oscillating pressurization in the gaps*

The dimensions of the gaps and the nature of the gases may cause an oscillating pressurization, such as illustrated in Fig. 8.

Hence, in addition to the problem of a propellant grain subjected to a pressure gradient $\Delta p(t) = P_c(t) - P_i(t)$—identical to case (a)—there is a

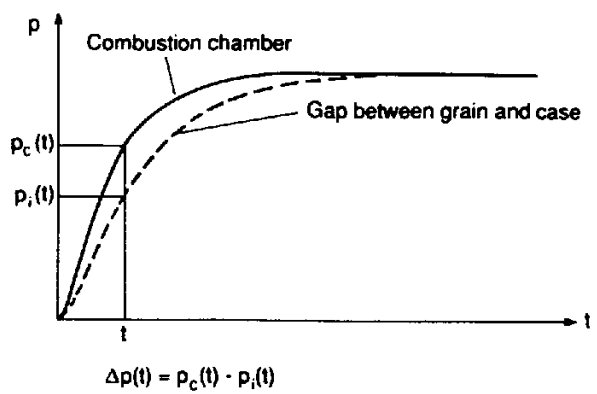


FIG. 6.7. Pressure rise induced by firing in a free-standing propellant.

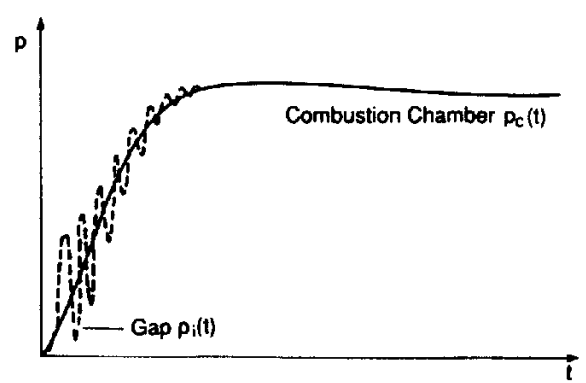


FIG. 6.8. Oscillating pressure rise induced by firing in a free-standing grain.



dynamic coupling between the propellant grain and the gases in the gap. This is a very complex problem to resolve because the dimensions of the gap evolve continuously, modifying the pressure rise conditions. An initial approach consists in making sure that a natural frequency of the grain does not correspond to the oscillation frequency of the pressure in the gap.

The mechanical loads described in the preceding section are usually the most significant factors in the structural design analysis. Yet, during the service life of rocket motors, other stresses/strains may appear that influence the structural integrity of the propellant grains. These include dynamic loads, typically shocks. These mechanical stimuli are not included in this chapter.

The grain structural analysis allows the clear identification of the parameters necessary to determine the margin of safety. These are:

- the temperature of the propellant;
- the pressure in the combustion chamber;
- the loading rate;
- the loading time.

They are used to calculate the boundary conditions, the behavior laws, and the capability of the materials.

## 3. Some Generalities and Definitions

### 3.1. STRESSES AND STRAINS

An object which is subject to mechanical loading (stresses or displacements applied to the external surfaces) finds a new state of equilibrium after the deformation has taken place. In each point $M$ of this object, there is an infinity of forces applied to the infinity of planes traversing this point (Fig. 9a).

In relation to a $P_1$ plane, on a $dS_1$ surface element, a $d\vec{F}_1$ force is applied; in relation to a $P_2$ plane, on a $dS_2$ surface element, a $d\vec{F}_2$ force is applied.

For each of the planes, the $d\vec{F}$ forces are the sum of a component $dF_n \cdot \vec{n}$, normal to the plane, and a component $dF_t \cdot \vec{t}$, contained in the plane:

$$d\vec{F} = dF_n \cdot \vec{n} + dF_t \vec{t}$$

The stresses applied to each plane are defined by the following equations:

$$\sigma_n = \lim_{dS \to 0} \frac{dF_n}{dS}, \quad \tau = \lim_{dS \to 0} \frac{dF_t}{dS}$$

Consequently, there is an infinity of stresses at each point of an object subjected to mechanical loading. The stress state is defined by a matrix composed of nine components expressed in a given perpendicular axis system. We use the term "stress tensor."

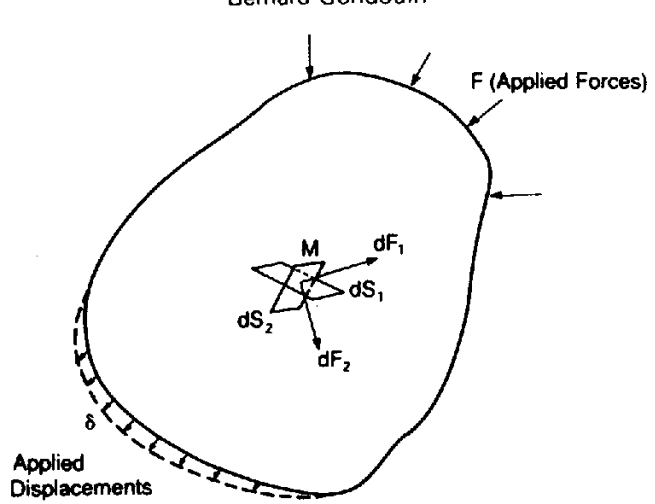


FIG. 6.9a. Description of forces in one point of a body at equilibrium.

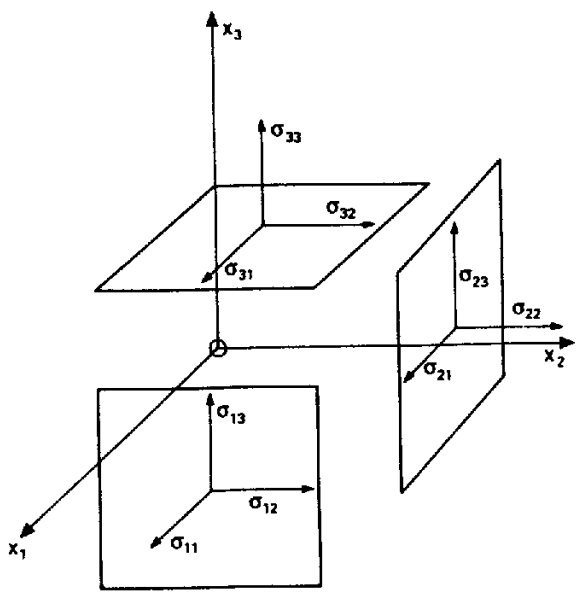


FIG. 6.9b. Description of the tensor component at one point of a body in equilibrium.

Similarly, a strain tensor is defined for each point; if $u_1$, $u_2$ and $u_3$ are three components in a reference system $(Ox_1, x_2, x_3)$ of the displacement of the $M$ point, the nine strain components expressed in the reference system are written:

$$\varepsilon_{ij} = \frac{1}{2}\left(\frac{\partial u_i}{\partial x_j} + \frac{\partial u_j}{\partial x_i}\right) \quad i, j, 1 \text{ to } 3$$



## 3.2. BEHAVIOR LAW: THE NECESSARY COEFFICIENTS TO BE DETERMINED

To know the behavior of a material is to determine the law relating the stress tensor to the strain tensor when the material is subjected to mechanical loading. For each point, there is a relation:

$$\sigma_{ij} = \mathcal{C}_{ijkl} * \varepsilon_{kl}$$

stress tensor = behavior * strain tensor.

In its general form the behavior of a material is rather complex; it has been demonstrated, however, that in a material that is homogeneous, elastic and isotropic, the definition of the behavior is limited to two coefficients, which are:

- the Lamé coefficients $\lambda$, $\mu$;
  or
- Young's modulus and Poisson's ratio, $E$ and $\nu$;
  or
- the shear modulus and the bulk modulus, $G$ and $K$.

For infinitesimal strains there are equations between these three pairs of coefficients (Table 1).

TABLE 1

| | | Function of | | |
|---|---|---|---|---|
| | | $\lambda$ and $\mu$ | $E$ and $\nu$ | $G$ and $K$ |
| Lamé's coefficients | $\lambda$ | | $\frac{E\nu}{(1+\nu)(1-2\nu)}$ | $K - \frac{2}{3}G$ |
| | $\mu$ | | $\frac{E}{2(1+\nu)}$ | $G$ |
| Young's modulus | $E$ | $\frac{\mu(3\lambda+2\mu)}{\lambda+\mu}$ | | $\frac{9KG}{3K+G}$ |
| Poisson's ratio | $\nu$ | $\frac{\lambda}{2(\lambda+\mu)}$ | | $\frac{3K-2G}{2(3K+G)}$ |
| Shear modulus | $G$ | $\mu$ | $\frac{E}{2(1+\nu)}$ | |
| Bulk modulus | $K$ | $\lambda + \frac{2}{3}\mu$ | $\frac{E}{3(1-2\nu)}$ | |

One or the other of these pairs of coefficients can be used indifferently. In any Cartesian coordinates $(x_1, x_2, x_3)$, the stress tensor and the strain tensor at an $M$ point are expressed by the following six components:

for the stress tensor (Fig. 9b):

$$\sigma_{11}, \sigma_{22}, \sigma_{33}, \sigma_{12} = \sigma_{21}; \sigma_{13} = \sigma_{31}; \sigma_{23} = \sigma_{32}$$

for the strain tensor:

$$\varepsilon_{11}, \varepsilon_{22}, \varepsilon_{33}, \varepsilon_{12} = \varepsilon_{21}, \varepsilon_{11} = \varepsilon_{31}, \varepsilon_{23} = \varepsilon_{32}$$

The equations between stress and strain are then written as:

*with E and ν*:

$$\begin{cases} \varepsilon_{11} = \dfrac{1}{E}(\sigma_{11} - \nu(\sigma_{22} + \sigma_{33})) \\ \varepsilon_{22} = \dfrac{1}{E}(\sigma_{22} - \nu(\sigma_{11} + \sigma_{33})) \\ \varepsilon_{33} = \dfrac{1}{E}(\sigma_{33} - \nu(\sigma_{11} + \sigma_{22})) \\ \varepsilon_{12} = \dfrac{1+\nu}{E}\sigma_{12}; \varepsilon_{13} = \dfrac{1+\nu}{E}\sigma_{13}; \varepsilon_{23} = \dfrac{1+\nu}{E}\sigma_{23} \end{cases} \quad (1)$$

*with λ and μ*:

$$\sigma_{ij} = 2\mu\varepsilon_{ij} + \delta_{ij}\lambda e \qquad i \text{ and } j \text{ vary from 1 to 3} \quad (2)$$

with

$$e = \varepsilon_{11} + \varepsilon_{22} + \varepsilon_{33}$$

$$\delta_{ij} = \begin{cases} 0 & i \neq j \\ 1 & i = j \end{cases} \qquad \text{the Kronecker symbol}$$

*with G and K*:

Any condition of stress, expressed by one of the equations described above, can be written as follows:

$$\sigma_{ij} = \sigma'_{ij} + \delta_{ij}\bar{\sigma} \quad i \text{ and } j \text{ vary from 1 to 3} \quad (3)$$

with

$\bar{\sigma} = \frac{1}{3}(\sigma_{11} + \sigma_{22} + \sigma_{33})$

$\delta_{ij}$ Kronecker symbol

$\bar{\sigma}$ is the mean stress or mean pressure

$\sigma'_{ij}$ are the deviatoric stresses.



In parallel, the strain can be written under the same form, i.e. the equation:

$$\varepsilon_{ij} = \varepsilon'_{ij} + \delta_{ij}\frac{e}{3}$$

The stress-strain equations are therefore written as:

$$\begin{aligned} \sigma'_{ij} &= 2G\varepsilon'ij \quad \text{6 equations for the deviatoric components} \\ \bar{\sigma} &= Ke \quad \text{1 equation for the isotropic component} \end{aligned} \quad (4)$$

The isotropic component represents the behavior of material subjected to a uniform load. For example, an isotropic object subjected to hydrostatic pressure shows a uniform strain. The deformation of the object is the same in all directions, and there is no shear effect.

The equations for the deviatoric components represent the behavior in the case of a non-uniform loading, where shear effects occur.

These two types of behavior involve different physical mechanisms. It is for that particular reason that during the behavior analysis of propellants, as well as for the stress/strain analysis in a propellant grain, this formulation is sometimes called upon, even though Young's modulus and Poisson's ratio are traditionally used.

*General comment.* The components of the stress tensors and strain tensors are expressed within the coordinate system. It is obvious that an object subjected to mechanical loading is in equilibrium with a stress and strain state which is independent of the coordinate system by which the components are expressed. The notion of a tensor invariant is used in this case. The first three invariants of the stress tensor and of the strain tensor are $S_1$, $S_2$ and $S_3$ for the stress, and $I_1$, $I_2$ and $I_3$ for the strain.

$S_1 = \sigma_{11} + \sigma_{22} + \sigma_{33}$

$S_2 = \sigma_{11} \cdot \sigma_{22} - \sigma_{12}^2 + \sigma_{22}\sigma_{33} - \sigma_{23}^2 + \sigma_{33}\sigma_{11} - \sigma_{13}^2$

$S_3$ = the determinant of the matrix of the stress tensor coefficients.

These values are independent of the coordinate system selected; only a function of these values can be used to represent the stress or strain states of an object.

## 3.3. TESTS DESIGNED TO DETERMINE THE COEFFICIENTS

All that is needed to know the behavior of a material is the determination, through simple tests, of one of the three coefficient pairs described above. In practice, relations (1) and (4) alone are used.

### 3.3.1. Determination of E and ν

In the following example we assume a parallelepipedic object with one dimension greater than the other two (Fig. 10).

When this object is subjected to a force $\vec{F}$ in the direction of its greatest dimension ($Ox_1$ in Fig. 10), the stress and strain induced in the material are:

$\sigma_{11}$ and $\varepsilon_{11}$ in the $Ox_1$ direction
$\sigma_{22}$ and $\varepsilon_{22}$ in the $Ox_2$ direction
$\sigma_{33}$ and $\varepsilon_{33}$ in the $Ox_3$ direction.

The only measurable physical values are the force applied and the deformation of the object.

On a surface that is free to deform itself the stress is equal to zero. Since the dimension of the object in the $Ox_2$ and $Ox_3$ directions is very small, the following can be written: $\sigma_{22} = \sigma_{33} = 0$.

Calling $\Delta l_1$, $\Delta l_2$, and $\Delta l_3$ the variations of the dimensions of the specimen, the stress and strain are written as follows:

$$\sigma_{11} = \frac{F}{S_0} \quad \varepsilon_{11} = \frac{\Delta l_1}{l_1}$$
$$\sigma_{22} = 0 \quad \varepsilon_{22} = \frac{\Delta l_2}{l_2} \tag{5}$$
$$\sigma_{33} = 0 \quad \varepsilon_{33} = \frac{\Delta l_3}{l_3}$$

Equation (1) enables us to write:

$$\varepsilon_{11} = \frac{1}{E}(\sigma_{11} - \nu(\sigma_{22} + \sigma_{33})) = \frac{\sigma_{11}}{E}$$
$$\varepsilon_{22} = \frac{1}{E}(\sigma_{22} - \nu(\sigma_{11} + \sigma_{33})) = \frac{\nu\sigma_{11}}{E} = -\nu\varepsilon_{11}$$
$$\varepsilon_{33} = -\nu\varepsilon_{11}$$

$E$ (Young's modulus) is obtained directly from the equation:

$$E = \frac{\sigma_{11}}{\varepsilon_{11}} = \frac{F}{l_2 l_3} * \frac{l_1}{\Delta l_1} \tag{6}$$

and similarly, Poisson's ratio $\nu$ is written:

$$\nu = -\frac{\varepsilon_{22}}{\varepsilon_{11}} = -\frac{\Delta l_2}{\Delta l_1} \times \frac{l_1}{l_2} \tag{7}$$



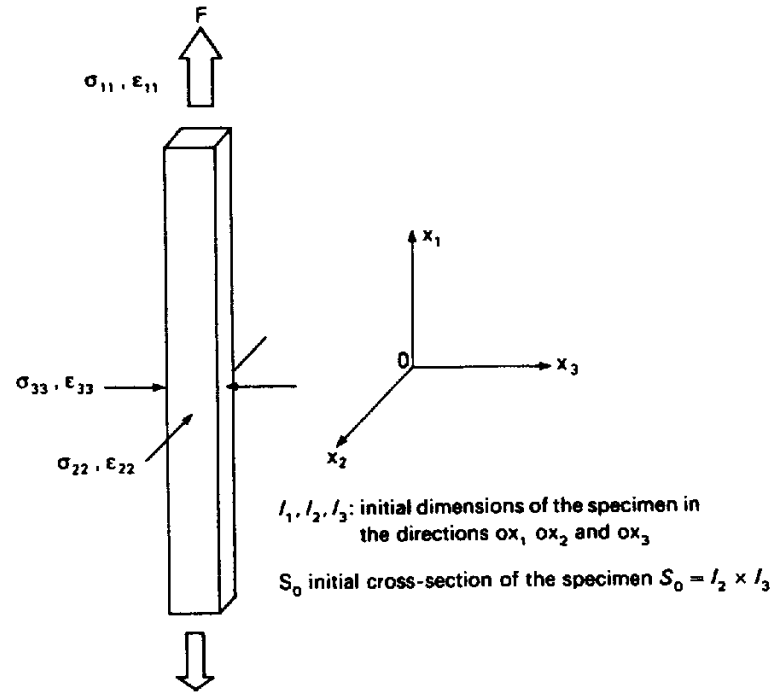


FIG. 6.10. Uniaxial tensile test specimen.

This parallelepipedic object is a unidimensional specimen. Its dimensions may vary. In Fig. 11 several unidimensional specimens used to analyze the behavior of propellants are described.

*Comment.* When analyzing the results of tests performed on propellant grains which show a great deal of deformation, the use of eqns (5) to predict the stress and strain is no longer valid. Indeed, when the changes of the dimensions of the specimen are no longer small compared to the initial dimensions themselves, the assumption of infinitesimal deformation is no longer valid. It becomes necessary to use a specially designed mechanical model [22]. Using a model adapted to large-scale deformation is a very complex task; it requires a coherence between the methods of analysis of the tests and the methods of structural analysis. Among the many ways of performing the test analysis, the most widely used is as follows:

If $\sigma_{11}$ and $\varepsilon_{11}$ are the stress and the strain determined according to eqns (5), the corrected stress and strain are to be written as follows:

$$\sigma^c_{11} = \sigma_{11}(1 + \varepsilon_{11})$$
$$\varepsilon^c_{11} = \frac{\varepsilon_{11}}{1 + \varepsilon_{11}} \tag{8}$$

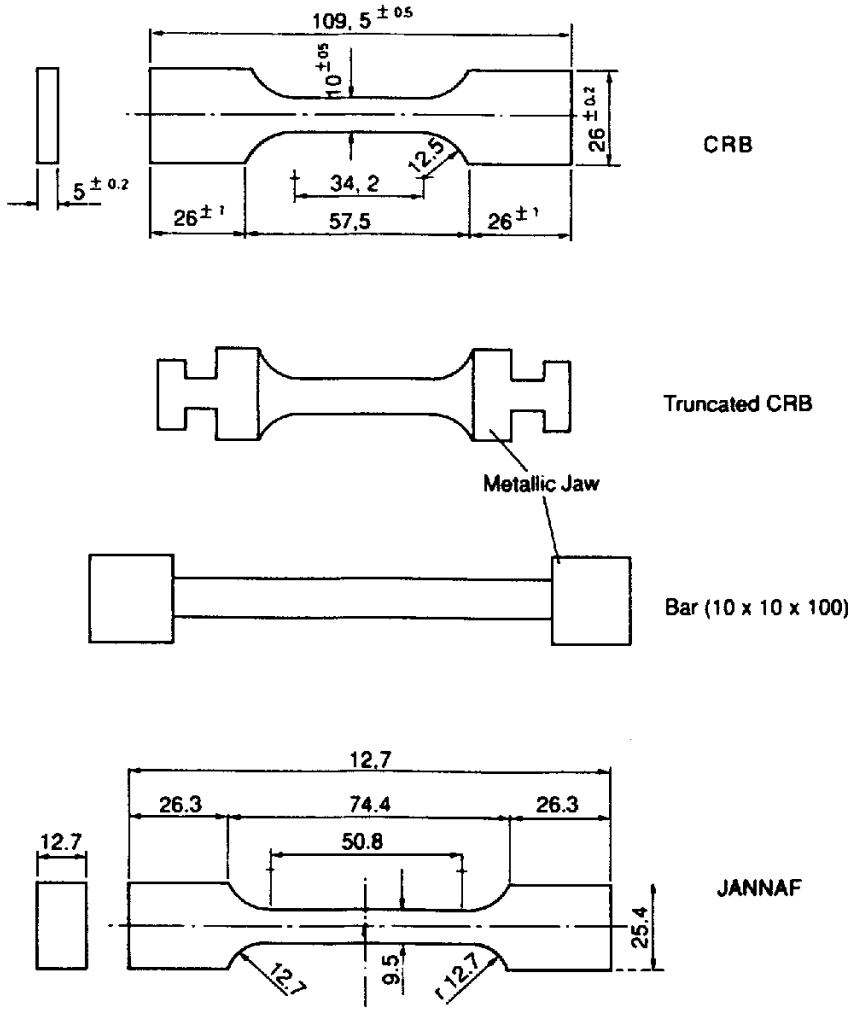


FIG. 6.11. Widely used uniaxial specimens.

### 3.3.2. *Determination of* K

The measurement of the bulk modulus is done simply by measuring the variation in the volume of an object of any shape subjected to hydrostatic pressure. Based on eqn (4):

$$\bar{\sigma} = Ke$$



for a material that exhibits little strain, $e$ corresponds to the change in volume.

$\bar{\sigma}$ is equal to the pressure applied.

### 3.3.3. *Determination of* G

Knowing $E$, $\nu$ and $K$ makes it possible to calculate $G$ using the relations existing between the various coefficients. There are, however, specific specimens with which the shear modulus $G$ can be directly determined. These are the torsional stress or shear specimens shown in Fig. 12.

Uniaxial specimens (Fig. 11) are widely used for a variety of tests (Fig. 13):

- tensile tests (induced displacements);
- relaxation tests (constant strain);
- creeping tests (constant stress load);
- combined tests: (a) loading-relaxation-loading (LRL); (b) loading-unloading-loading (LUL)

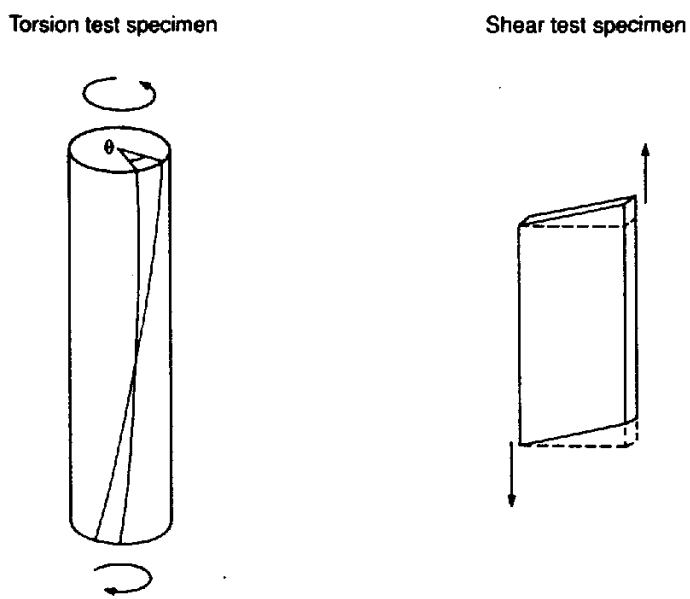


FIG. 6.12.

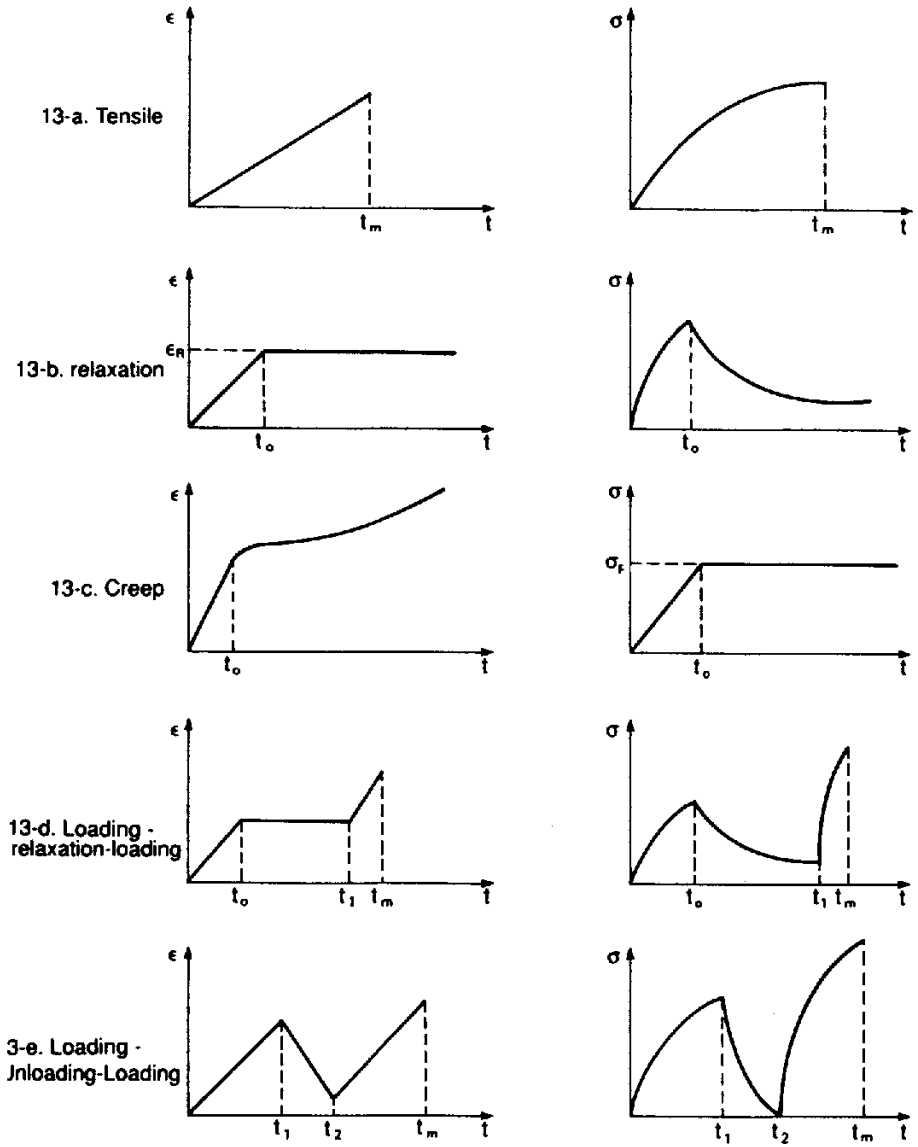


FIG. 6.13. Description of the various types of tests.

These tests are performed under various:

- temperatures;
- pressures;
- loading rates for the tensile tests, and durations for the relaxation and creeping tests.



## 3.4. VARIOUS TYPES OF BEHAVIORS OF THE MATERIALS

To determine the behavior law of a material, it is necessary to perform combined tests, such as loading-relaxation-loading or loading-unloading-loading types of tests. Tensile tests alone are not sufficient to draw conclusions on the behavior type of a material. For example, the results of a tensile test listed in Fig. 14 can be obtained from materials whose structural integrity is different, which can only be discovered through combined tests (Fig. 15).

In solid mechanics there are only two types of behavior:

- elastic or elastoplastic, where the rate of loading and the duration play no role;
- viscoelastic or viscoplastic, where the rate of loading and the duration modify the response of the material.

The behavior, for each of these families, may be either linear or non-linear, since linearity satisfies the rules of homogeneity and additivity.

*Homogeneity*

$$\text{if} \quad \varepsilon_{ij}(t) \to \sigma_{ij}(t) \qquad (9)$$
$$\text{then} \quad k\varepsilon_{ij}(t) \to k\sigma_{ij}(t)$$

where $k$ is any constant.

*Additivity*

$$\text{if} \quad \varepsilon^1_{ij}(t) \to \sigma^1_{ij}(t)$$
$$\text{and if} \quad \varepsilon^2_{ij}(t) \to \sigma^2_{ij}(t)$$
$$\text{then} \quad \varepsilon^1_{ij}(t) + \varepsilon^2_{ij}(t) \to \sigma^1_{ij}(t) + \sigma^2_{ij}(t)$$

To determine the response of a material under induced stress and strain, it is desirable first to determine the structural behavior type (elastic, plastic, viscoelastic, and linear or non-linear); and second to select the tests best suited for the future applications of the material and for the measurement of its mechanical coefficients.

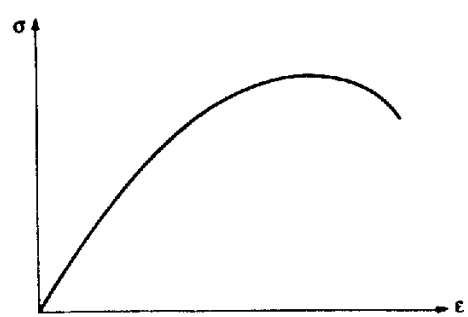


FIG. 6.14. Result of a classic tensile test.

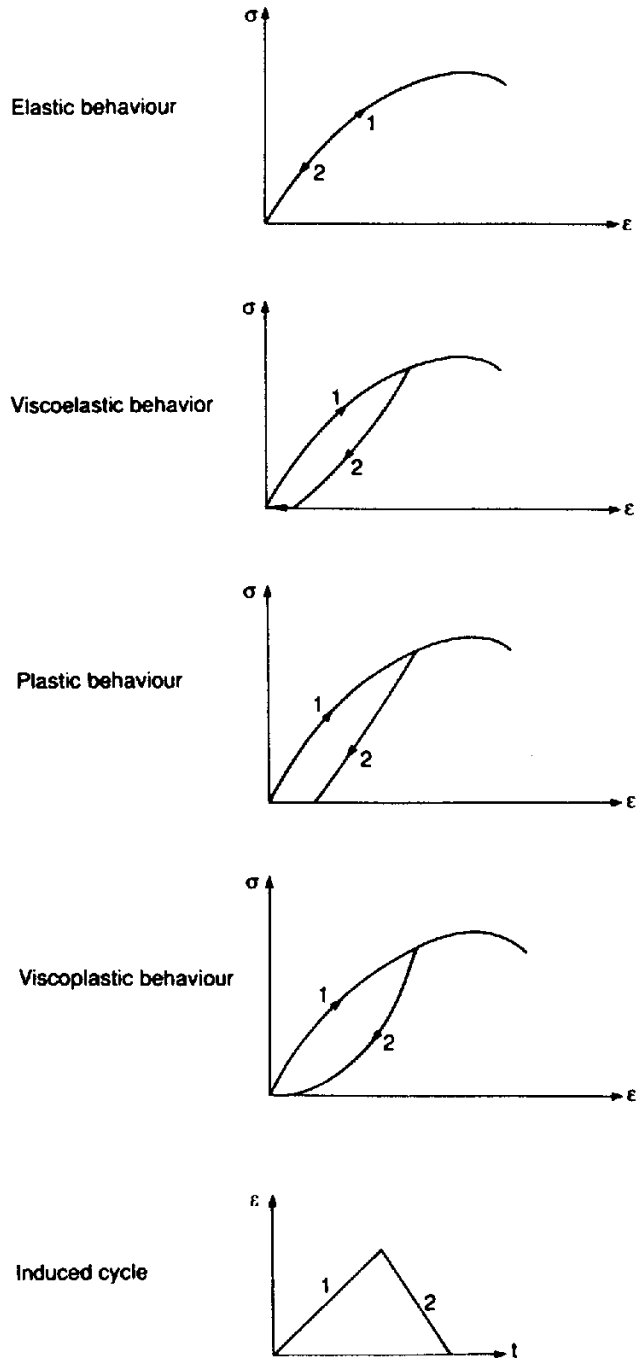


FIG. 6.15. The various types of behavior for the same tensile curve.



# 4. Structural Properties of Propellants and Their Bonding

## 4.1. PHYSICAL DESCRIPTION OF PROPELLANT

### *4.1.1. Composite and composite modified double-base propellants (Chapters 10 and 11)*

Composite propellants consist of small-particle-size solids in a polymeric matrix. The loading ratios are, typically, very high (sometimes greater than 70% of the volume). The bonding surfaces between the binder and the fillers are very important. When relatively low rate structural loading is induced ($\dot{\varepsilon} < 1\ s^{-1}$), there is failure of the bonding between some fillers and the binder, or failure of the binder close to a solid particle. Vacuum holes are created, and their size increases with the stress/strain. This phenomenon generates a dissipation of energy resulting in a viscous behavior, at a macroscopic scale to which is eventually added the viscous nature inherent to the binder.

When these vacuum holes reach a significant size (several microns) they act as microfailures initiating small cracks in the binder, and causing failure of the propellant grain.

These phenomena correspond to two clearly distinct phases (Fig. 16).

- *Stress/strain of the bonding between the binder and the fillers.* It is the structural properties of the binder and of the bonding that govern the mechanical behavior of the propellant. The total solids content, their

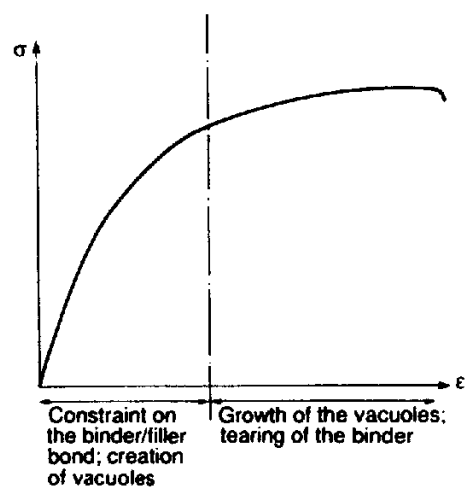


FIG. 6.16. Tensile test on a composite propellant.

shape, and particle size distribution influence the propellant behavior by affecting the bonding properties.

- *Growth of the microfailures (vacuum holes).* It is the tearing characteristics of the binder, as well as the total solids content and their size distribution which rule the structural behavior up to the failure of the propellant grain.

The behavior type of these propellants is determined by performing the LRL or LUL tests. The aspect of the curves obtained (Fig. 17) indicates a non-linear viscoelastic behavior.

*Comment.* Some composite propellants have a perfectly elastic binder. Since the fillers themselves are also elastic, their viscous structural behavior is due solely to the dissipation of energy at the bonding level between the binder and the solids.

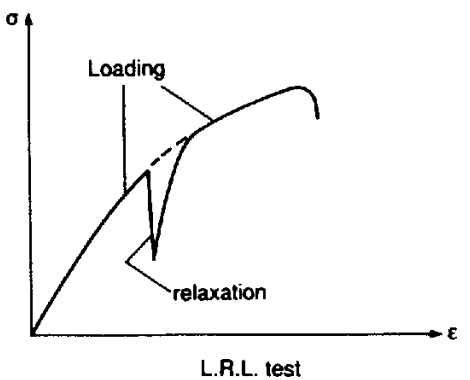


FIG. 6.17. L.R.L. and L.U.L. tests on composite propellant.



### 4.1.2. *Double-base propellant grains*

The double-base propellant grains are gels containing at least two main ingredients: nitrocellulose and nitroglycerine. According to the various manufacturing methods, there are two main families (Chapter 9):

- solventless double-base propellants (also called extruded double-base propellant EDB);
- cast double-base propellants (CDB).

These are homogeneous propellants from the aspect of structural mechanical properties; but their production process may cause anisotropies, for instance in EDB propellants.

Their physical structure looks like a solid phase (nitrocellulose), consisting of a continuous tridimensional network inside of which there is a liquid phase (nitroglycerine).

Usually, this structure leads to materials which are more rigid than the composite propellants, but when mechanical loading is imposed, the presence of the two distinct phases causes energy dissipations resulting in a more or less pronounced viscous behavior.

*Comment.* Crosslinked double-base propellants (Chapter 11) have some of the characteristics of the double-base propellants: the binder has the physical structure of a gel, which is crosslinked. They are, nevertheless, ranked as composite propellants insofar as the solids content ratio is such that the bonding phenomena between the binder and the solids are the predominant factors and govern the behavior of the propellant.

## 4.2. MECHANICAL BEHAVIOR OF THE PROPELLANTS

Each type of propellant has its own specific mechanical characteristics. Still, the methods used to determine their behavior are identical for every one of them, and the influence of the various parameters (temperature, pressure, loading rate) is the same overall for all propellants. Consequently, distinctions will no longer be made between each type of propellant in the following sections of this chapter.

### 4.2.1. *Tensile behavior*

The tensile tests are widely used for the fine analysis of the propellants' behavior as well as for the manufacturing controls of these propellants. Because their behavior is not linear elastic, it is necessary to define a certain number of parameters that allow a better representation of the aspects of the experimental curves. These parameters, shown in Fig. 18, are:

$E$ Young's modulus, or tangent modulus, or initial modulus;
$\sigma_m$ maximum stress;

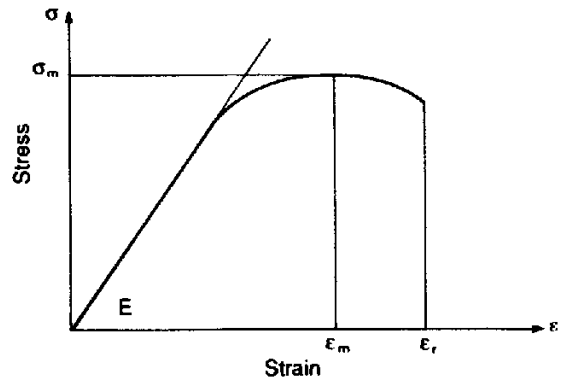


FIG. 6.18. The various parameters describing a typical curve.

$\varepsilon_m$ strain at maximum stress;
$\varepsilon_r$ strain at rupture.

The capability, as defined above in Section 1, for a tensile test is expressed by the maximum stress $\sigma_m$, and the strain $\varepsilon_m$, or by any other function taking these two parameters into consideration.

When the aspect of the tensile curve differs from the curve shown in Fig. 18, other values need to be determined.

The values for the parameters defined above vary with each propellant type, and with the pressure, temperature, and loading rate parameters for each propellant. Age and humidity are also common factors which affect these parameters.

When it is used in the case-bonded form, the propellant must exhibit the greatest possible $\varepsilon_m$ during the thermal cycle and at the time of firing. On the other hand, maximum stress, $\sigma_m$ must be high for the stress induced by acceleration (gravity and flight of the missile).

The problem is different in the case of a free-standing grain, and in fact this type of configuration is selected for highly rigid propellants (high modulus $E$), with high $\sigma_m$ and low $\varepsilon_m$. For example, this is the case with double-base propellants.

During a tensile test the physical nature of the propellant (described in Section 4.1.) results in an increase of the volume of the specimen, caused by the occurrence of vacuum holes around some crystalline fillers, or by the increase of micro-cracks in double-base propellants. Knowledge of these phenomena contributes greatly to the determination of the behavior of the materials.

The simultaneous measurement of the volume dilation during a tensile test is done with a gas dilatometer developed by Farris [4]. The method consists in measuring the pressure variation in an enclosure where the specimen is



placed. The change of the pressure is directly linked to the volume dilation of the specimen.

The general aspect of the curves obtained is shown in Fig. 19.

Phases I, II and III of the behavior illustrated in Fig. 19 can be understood in the following manner:

Phase I The zero relative volume dilatation corresponds to an incompressible behavior.
Phase II Creation of vacuum holes or micro-cracks.
Phase III Size increase of the vacuum holes and micro-cracks.

The $\varepsilon_d$ value is also called dewetting strain; it identifies the threshold above which the propellant is no longer incompressible. For composite propellants, the higher its value, the better the bonding between the binder and the oxidizers will be. It is a characteristic indicative of good structural integrity of the propellants. $\varepsilon_d$ depends on temperature, loading rate, and pressure imposed.

As a rule, $\varepsilon_d$ increases with the temperature, or when the loading rate decreases, or again when the pressure increases.

It is difficult to assign values to the dewetting elongation, since this parameter may take different values for each propellant with the pressure ($p$) temperature ($T$) and loading rate ($\dot{\varepsilon}$) parameters. For composite propellants with a 20°C temperature, at atmospheric pressure, and a $\dot{\varepsilon}$ loading rate of the order of $10^{-2}\,s^{-1}$, $\varepsilon_d$ is usually comprised between 7 and 12%.

$\alpha$, the angle formed by the asymptote with the axis of the strains, corresponds to the quantity of vacuum holes or micro-cracks present in the propellant. The smaller the number of cavities in the propellant, the smaller $tg\alpha$ is (a favorable characteristic). As in the case of $\varepsilon_d$, $tg\alpha$ varies with the three $p$, $T$, and $\dot{\varepsilon}$ parameters. As a rule, $tg\alpha$ decreases when the pressure increases, when the temperature increases or when the loading rate decreases.

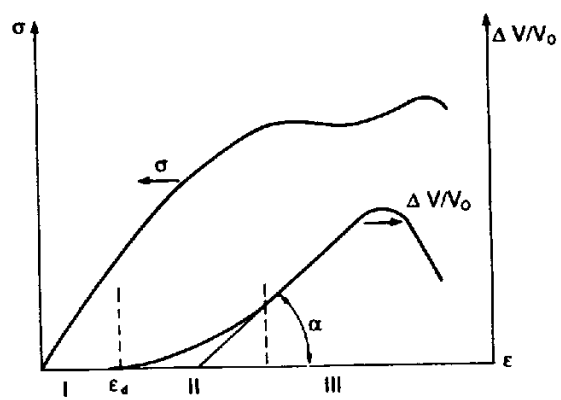


FIG. 6.19. The three behavior phases of a propellant. During a tensile test with measurement of the volume dilatation.

In composite propellants $tg\alpha$ must be as low as possible, but the selection of the propellants must be primarily based on a dewetting strain that is as high as possible.

A particularly interesting test, which is derived from the tensile test, consists in varying the temperature of the propellant specimen during a low-speed tensile test. This test corresponds to the stress imposed on the propellant in a case-bonded propellant subjected to a temperature drop.

The stress response is illustrated in Fig. 20.

Given $T_f$ as the temperature at rupture of the specimen; the elongation at break obtained during a tensile test with simultaneous cooling is much higher than for a tensile test performed at a constant $T_f$ temperature and identical loading rate.

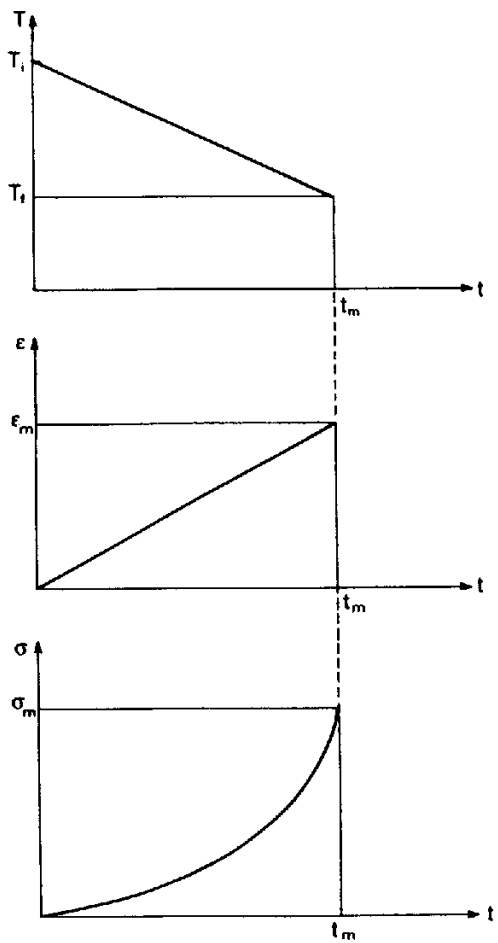


FIG. 6.20. Tensile test with simultaneous cooling of the specimen.



Results of tests performed with propellants under various testing conditions are given in the table and diagram in Fig. 21. Of great interest is the fact that when a case-bonded propellant is cooled down, the $e_m$ elongation capability depends on the way the cooling-down is handled. Figure 21 shows the evolution of this parameter as a function of the ratio of the loading rate to the cooling-down rates. For a given propellant, subjected to a cool-down, there is a corresponding value of the $\Delta\varepsilon/\Delta T$, and a maximum allowable elongation value corresponds to that ratio.

### 4.2.2. *Stress relaxation and creep*

The viscous nature of the mechanical behavior of a propellant is demonstrated by relaxation and creep tests.

The relaxation test, which consists in subjecting a specimen to a constant elongation and in measuring the evolution of the stress, corresponds to the mechanical load existing in a case-bonded propellant stored at a constant temperature, below the curing temperature.

| T in °C/h | $V_T$ in mm/min | $T_f$ °C | $E_m$ in % | $\sigma_m$ in MPa | $\lvert\frac{\Delta\varepsilon}{\Delta T}\rvert$ %/°C |
|---|---|---|---|---|---|
| -10 | 0,05 | -72 | 55 | 13,5 | 0,6 |
| -10 | 0,1 | -67,5 | 105 | 6,3 | 1,2 |
| -5 | 0,05 | -70,8 | 109 | 7,8 | 1,2 |
| -20 | 0,1 | -70 | 54 | 9 | 0,6 |
| -7 | 0,1 | -65,8 | 147 | 4,5 | 1,71 |
| T = - 60°C | 0,1 | | 11,4 | 12 | isothermal tensile test |

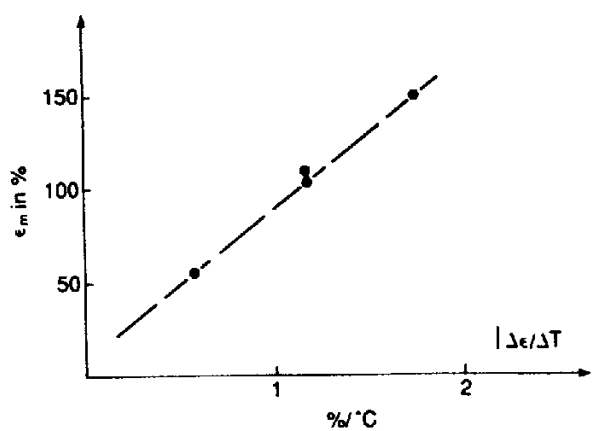


FIG. 6.21. Results of tensile test with simultaneous cooling.

The creep test consists of subjecting a specimen to a constant load and in measuring the evolution of the elongation. This test corresponds to the mechanical loading induced into propellants subjected to a constant acceleration.

### *(a) Relaxation*

In a relaxation test performed on an uniaxial specimen, if $\varepsilon_i$ is the constant elongation prescribed during the test, and if $\sigma(t)$ is the evolution of the stress versus time which is measured, the relaxation modulus $E_R(t)$ is expressed by:

$$E_R(t) = \frac{\sigma(t)}{\varepsilon_i} \tag{11}$$

Similarly, in a creeping test, the compliance $J(t)$ is expressed by:

$$J(t) = \frac{\varepsilon(t)}{\sigma_i} \tag{12}$$

The compliance is the inverse of a modulus.

The shape of the relaxation modulus $E_R(t)$ looks like the illustration in Fig. 22.

For the propellants, the relaxation modulus usually depends on the temperature and the strain level. For an identical amount of time, the relaxation modulus decreases when the temperature increases, or when the strain level increases (Fig. 23).

When the variation in the relaxation modulus versus the strain level is small, a linear viscoelastic law can be used. At a given temperature, the curve plotted on Fig. 22 can be written using one of the following forms:

*Homographic form*

$$E_R(t) = E_1 + \frac{E_2}{\left(1 + \frac{t}{\tau}\right)^n} \tag{13}$$

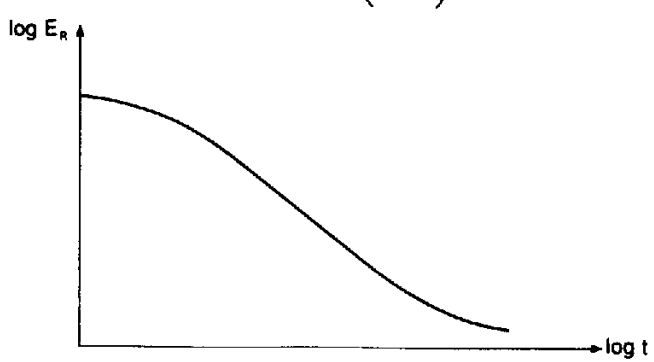


FIG. 6.22. Aspect of the relaxation modulus of composite propellants.



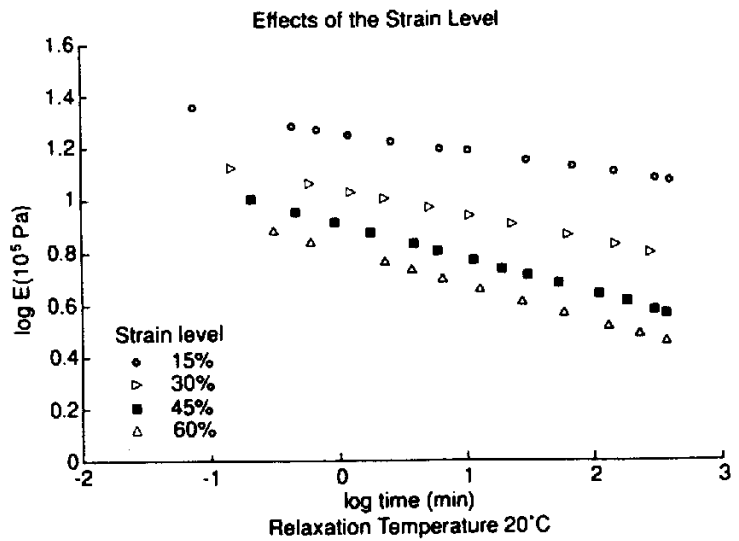


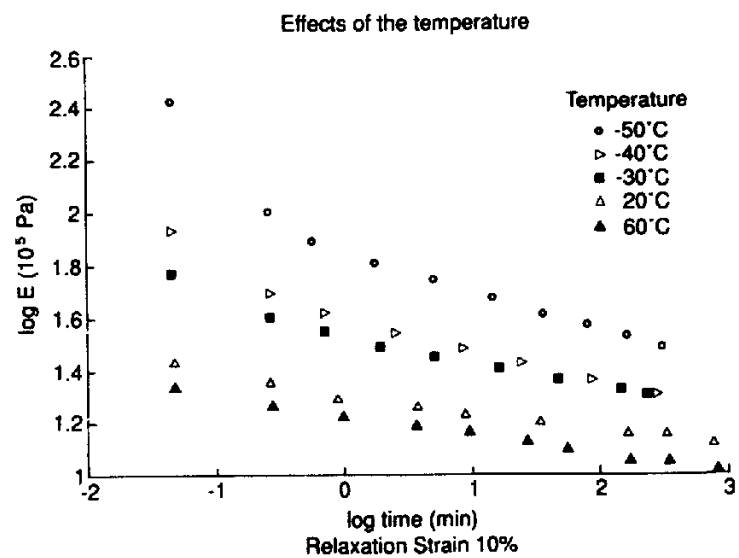


FIG. 6.23. Effects of the temperature and of the level of elongation on the relaxation modulus.

$E_1$, $E_2$, $\tau$ and $n$ are characteristic constants of the material that are determined experimentally.

*Prony series*

$$E_R(t) = E_0 + \sum_{i=1}^{N} E_i e^{-t/\tau_i} \tag{14}$$

$E_0$, $E_i$ and $\tau_i$ are characteristic constants of the material that are determined experimentally.

When tests are performed on an uniaxial specimen, the stress is expressed by the relation [2,3]:

$$\sigma(t) = E_R(t)\varepsilon(o) + \int_o^t E_R(t-\tau)\frac{\partial \varepsilon}{\partial \tau} d\tau \tag{15}$$

This form is valid only for a linear viscoelastic behavior.

In the case of non-linear behaviors, some authors propose using the same form as (15) by expressing the relaxation modulus into the product of two terms.

$$E_R(t, \varepsilon) = E_{R1}(\varepsilon)E_{R2}(t) \tag{16}$$

$E_{R1}(\varepsilon)$ may take the form of a polynomial.

Other authors propose laws that are better suited to propellants [9]; Francis has done a comparison of the laws developed by various authors for solid propellants [13]. No model appears completely satisfactory, and major research work is still being done in this area [23].

### *(b) Creeping*

The creep test is used only to determine the failure characteristics of solid propellants. A constant load $\sigma_F$ is applied on a specimen; the time to failure $t_R$ is recorded (Fig. 24).

## 4.2.3. *The effect of the temperature; time–temperature equivalence*

When relaxation tests are performed (at a given elongation) at various temperatures, the curves representing the evolution of the relaxation modulus for each temperature are deducted one from the other by a shift factor versus time (Fig. 25). This observation is generally true in the case of polymers. There is an equivalence between time and temperature. In the case of the relaxation, we can write:

$$E_R(t_0, T_0) = E_R(t_1, T_1) = E_R(t_2, T_2)$$



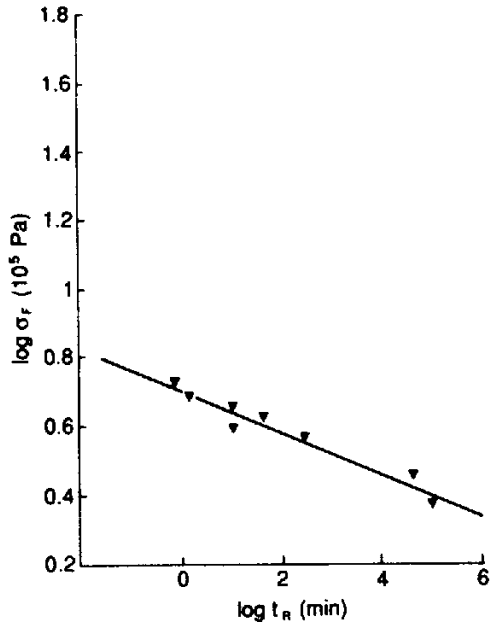


FIG. 6.24. Creep test: time to failure versus stress level.

where:

$$\log t_1 = \log t_0 + \log \mathbf{a}_{T_1}^{T_0}$$
$$\log t_2 = \log t_0 + \log \mathbf{a}_{T_1}^{T_0}$$

where $\mathbf{a}_{T_1}^{T_0}$ and $\mathbf{a}_{T2}^{T_0}$ are the shift factors, in relation to the $T_0$ reference temperature.

A sole curve can be identified, called the "master curve," which gives the value of the relaxation modulus versus a reduced time $t/\mathbf{a}_T^{T_0}$ for various temperatures. The corresponding time, called reduced time, is written as follows:

$$\xi = \int_0^t \frac{d\tau}{\mathbf{a}_T^{T_0}(T(\tau))}$$

The shift function is determined experimentally. Williams, Landel and Ferry [10] have developed an analytical form with two coefficients, $C_1$ and $C_2$, usually known as W.L.F. equation:

$$\log \mathbf{a}_T^{T_0} = \frac{-C_1(T - T_0)}{C_2 + T - T_0}$$

The reference temperature $T_0$ is often the ambient temperature, and the corresponding shift factor is written: $\mathbf{a}_T$.

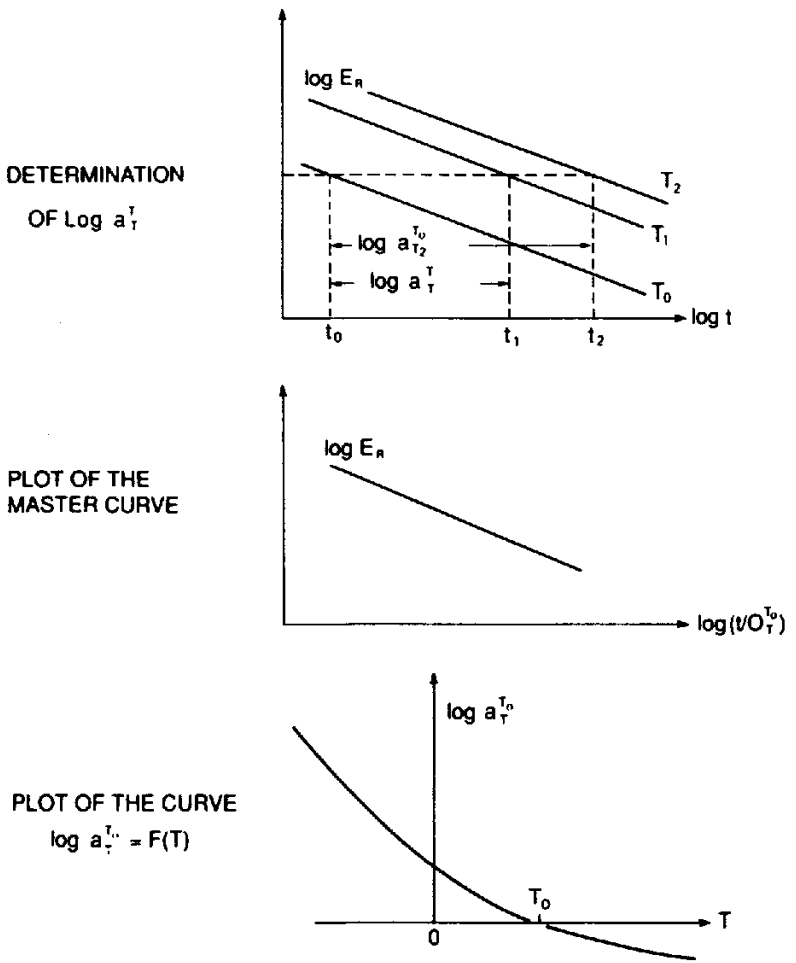


FIG. 6.25. Time-temperature equivalence.

Extending the concept, the principle of time-temperature equivalence is used on all characteristics measured experimentally during tensile tests:

- tangent modulus $E$;
- maximum stress $\sigma_m$;
- strain at maximum stress $\varepsilon_m$.

In the case of tensile tests it is an equivalence loading rate ($\dot{\varepsilon}$) - temperature that is used. The master curves are defined with the reduced variable $1/\dot{\varepsilon}a_T$.

$$\log E = f(\log 1/\dot{\varepsilon}a_T)$$
$$\log \sigma_m = g(\log 1/\dot{\varepsilon}a_T)$$
$$\log \varepsilon_m = h(\log 1/\dot{\varepsilon}a_T)$$



Time to failure at maximum stress $\sigma_m$ is:

$$t_m = \varepsilon_m/\dot{\varepsilon}$$

It becomes possible to plot the master curve under another form (Fig. 26).

$$\log \sigma_m = g'(\log t_m/a_T)$$

For some number of propellants, the shift factors measured on the moduli and on the maximum stresses are identical.

The time-temperature equivalence concept is empirical. Consequently, it must be determined for each propellant.

### 4.2.4. *Effect of the pressure*

It is necessary to know the effect of the pressure on the mechanical behavior of propellants as well as on their capability because, at the time of firing, the propellant grains operate under pressure. This pressure varies according to the propellant grains from 4 MPa to 15 MPa, and possibly higher.

Tests performed under pressure on specimens are done at constant pressure; the strain imposed on the propellant in a case-bonded grain is different, because the evolution of the stress and strain is due to the evolution of the pressure. To obtain the best possible simulation of the firing phenomena, it would be necessary to perform tensile tests with simultaneous pressure variation.

Qualitatively, during a tensile test, the effect of the pressure is to delay the occurrence of micro-cracks and vacuum holes. The relative variation in the

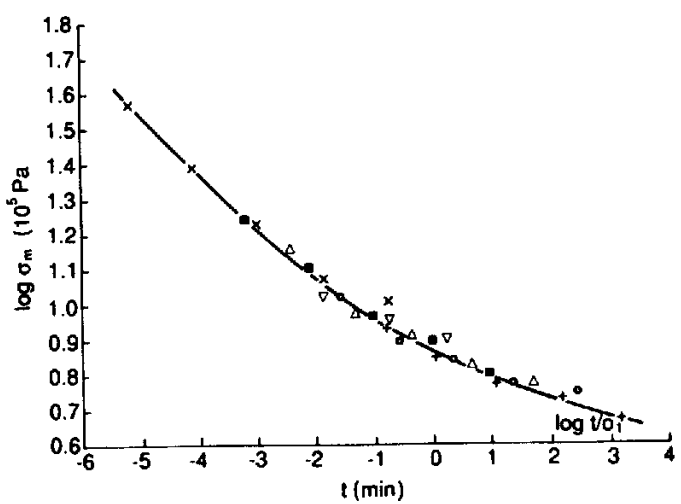


FIG. 6.26. Master curve of the maximum tensile stress.

volume that is measured during the test reveals an increase in the dewetting elongation and a decrease in $tg\alpha$.

The values of the maximum stress and corresponding strain are significantly increased in comparison with the values obtained at atmospheric pressure under the same temperature and strain rate conditions (Fig. 27, upper). For any common incompressible portion where the relative volume variation is zero, at atmospheric pressure and under pressure the propellant behavior is, of course, unchanged.

In the case of composite propellants with large elongations, and with a significant Phase III (shown in Fig. 19), the effect of pressure is generally described as follows (Fig. 27, lower).

*Phase I.* The propellant is incompressible, the amount of vacuum holes around the charges is low, possibly zero; the pressure has no effect on the behavior, and the tensile curves are identical for all pressures.

*Phase II* (of a test performed at atmospheric pressure). The number of vacuum holes increases and reaches maximum value at stress $\sigma_1$. The effect of the pressure is to delay the occurrence of the vacuum holes and to significantly decrease their number. With pressures of the order of 7 MPa, the number of vacuum holes stays very low until stress $\sigma_m^p$. Stress $\sigma_m^p$ and the corresponding elongation $\varepsilon_m^p$ must be compared to the strain at the end of Phase II, $\sigma_1$, and the corresponding elongation $\varepsilon_1$. The tensile behavior of highly filled composite propellants often exhibits only Phase I and II at atmospheric pressure. As a result, the comparison between the maximum stress and corresponding elongation presents no problem (Fig. 27, upper).

*Phase III* (of a test at atmospheric pressure). All vacuum holes have appeared; their number remains constant until stress $\sigma_m$. Their size increases between $\varepsilon_1$ and $\varepsilon_m$ and the difference between $\varepsilon_m$ and $\varepsilon_1$ is characteristic of the resistance to tearing of the binder. Under pressure, this phase may completely disappear. When micro-cracks appear in the binder, at a stress close to the maximum stress $\sigma_m^p$, which is much greater than the corresponding stress at atmospheric pressure ($\sigma_1$), the propagation of the cracks in the binder is much more rapid under pressure. Phase III is greatly reduced, sometimes practically nonexistent. It is therefore important to compare the corresponding stress and strain, respectively, because although the maximum stress of tests performed under pressure is typically greater than any stress experienced under tests at atmospheric pressure ($\sigma_m^p > \sigma_1$ and $\sigma_m^p > \sigma_m$), it is not true for elongations ($\varepsilon_m^p > \varepsilon_1$ and $\varepsilon_m^p < \varepsilon_m$).

The following question needs to be answered: which capability is to be taken into consideration? The effects described above increase when the pressure increases, up to a threshold pressure, after which the effects remain constant.



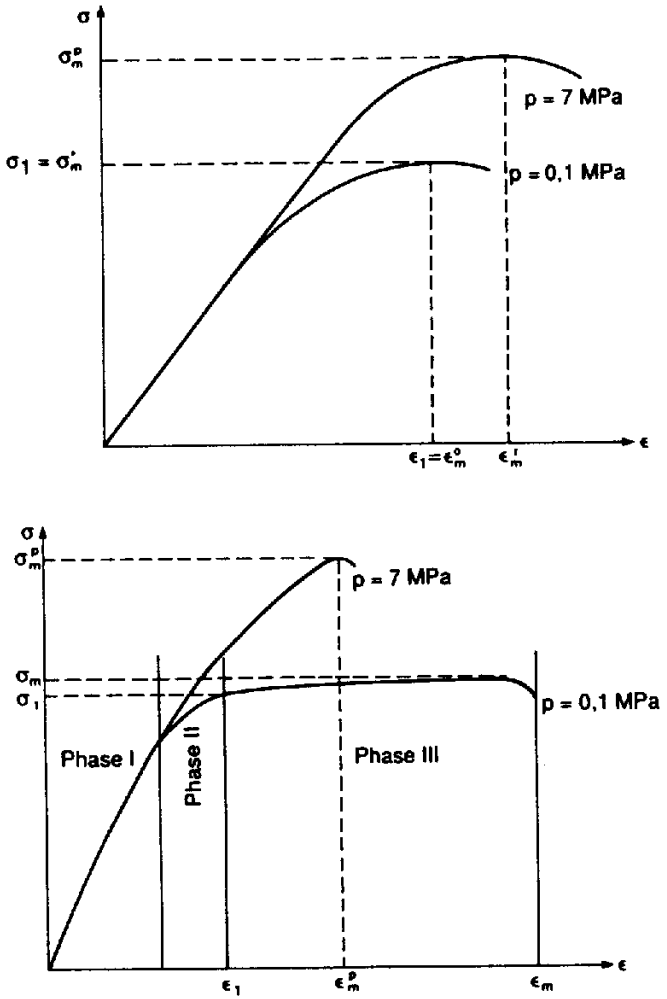


FIG. 6.27.

That threshold pressure depends on the materials, and for each propellant it depends on the rate of stress and the temperature. In fact, the higher the stiffness of the specimen, the greater the threshold pressure will be (Fig. 28).

### 4.2.5. *Behavior law of solid propellants*

Section 3.2 describes the coefficients that must be determined to know the mechanical behavior of the propellants.

All of the tests described above reveal a non-linear viscoelastic behavior, tricky to represent in a single model.

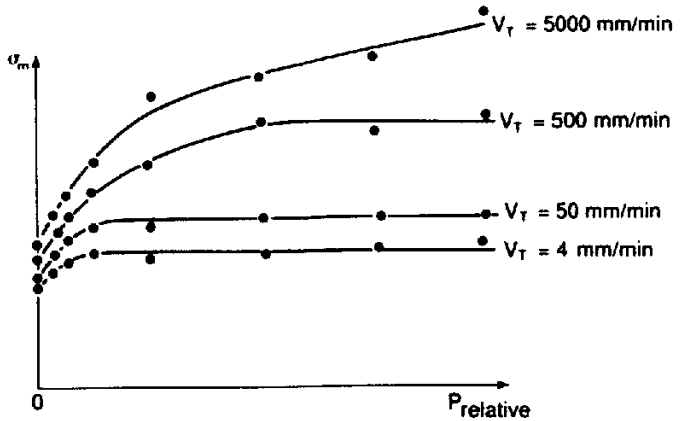


FIG. 6.28. Effect of the pressure on the maximum tensile stress.

The first important result is obtained during the tensile test with the simultaneous measurement of volume dilation. The volume dilation is zero up to elongation $\varepsilon_d$, which corresponds to incompressible behavior of propellants under small strains. Incompressibility, in the equations of mechanics, is a discontinuity which expresses itself by the fact that it is not possible to determine stress field from the strain field. The average stress $\bar{\sigma}$ depends on the geometrical confinement of the propellant.

Returning to the definition of the coefficients characteristic of the behavior, incompressibility is expressed by:

$$E \text{ (any)} \quad \nu \to 0.5$$

or $$G \text{ (any)} \quad K \to \infty$$

In fact, the bulk modulus has a finite value, but it is much greater than the shear modulus.

For that reason, relations (4) are used. In the case of a viscoelastic behavior, the formulation becomes:

$$\sigma'_{ij}(t) = 2G(t)\varepsilon'_{ij}(0) + 2\int_0^t G(t-\tau)\dot{\varepsilon}'_{ij}(\tau)\mathrm{d}\tau$$
$$\bar{\sigma}(t) = k\mathrm{e}(t) \tag{17}$$

where:

$\sigma'_{ij}(t)$ and $\varepsilon'_{ij}(t)$ are the deviatoric stress and strain tensors;
$\bar{\sigma}(t)$ is the average stress;
$\mathrm{e}(t) = 3\bar{\varepsilon}(t)$;
$\bar{\varepsilon}(t)$ is the average strain.



For infinitesimal strain, the volume dilatation is equal to $e(t)$. For an incompressible mechanical behavior, the relations between coefficients $E$, $\nu$ and $G$, $K$, become:

$$E = 3G; \quad \nu = \tfrac{1}{2} \tag{18}$$

Therefore, the relaxation modulus identified in Section 4.2.2 allows us to calculate easily the $G$ modulus, and the relation between the deviatoric tensors will be established simply. The relation between the average stress and the average strain is more complicated because, as a rule, $e(t)$ is very small and $K$ is very large. The methods used most widely to handle this problem are described in Section 5.

Propellants generally have a non-linear viscoelastic behavior. The laws used to model this type of behavior are mentioned in Section 4.2.2.

Starting with relation (17), which is valid for a linear behavior, an extension can be done by writing:

$$\sigma'_{ij}(t) = 2\int_0^t G(\varepsilon, t-\tau)\dot{\varepsilon}'_{ij}(\tau)\mathrm{d}\tau + 2G(\varepsilon, t)\varepsilon'_{ij}(0) \tag{19}$$

There have been other formulae proposed to model propellant behavior [13]. Farris [4], in particular, developed a theory that applies to composite propellants. This law is written:

*Deviatoric stress tensor*

$$\sigma'_{ij}(t) = \exp\{\beta I\gamma - \beta'(\Delta V/V_0)/I\gamma\}\left\{\left[G_1 + G_2\left(\frac{I_\gamma}{\|I_\gamma\|_{p_1}}\right)^{m_1}\right]\varepsilon'_{ij}(t) + G_3\left[1 - \left(\frac{I_\gamma}{\|I_\gamma\|_\infty}\right)^{m_2}\right]\int_0^t (t-\xi)^{m_3}\dot{\varepsilon}'_{ij}(\xi)\mathrm{d}\xi\right\} \tag{20}$$

$\sigma'_{ij}$ = deviatoric stress tensor
$\varepsilon'_{ij}$ = deviatoric strain tensor
$\Delta V/V_0$ = volume dilatation

if $\varepsilon_1, \varepsilon_2, \varepsilon_3$ are the principal strains

$$I_\gamma = \tfrac{1}{3}((\varepsilon_1-\varepsilon_2)^2 + (\varepsilon_2-\varepsilon_3)^2 + (\varepsilon_3-\varepsilon_1)^2)^{1/2} \quad \|I_\gamma\|_{p_1} = \left\{\int_0^t \frac{(I_\gamma)^{p_1}}{\mathbf{a}_T}\mathrm{d}\tau\right\}^{1/p_1}$$

$\mathbf{a}_T$ = shift factor of the time-temperature equivalence

$$\xi = \int_0^t \frac{\mathrm{d}\tau}{\mathbf{a}_T} \text{ is the reduced time}$$

$$\|I_\gamma\|_\infty = \max|I_\gamma|$$

$$G_1, G_2, G_3, \beta, \beta', m_1, m_2, m_3, p_1$$

are constants that are dependent on the material.

*Isotropic part*

$$\Delta V/V_0 = \frac{\bar{\sigma}}{K}\left[\exp\left\{\left[\chi_1 + \chi_2(T - T_0)\right]\bar{\sigma} - 1\right\}\right] + AI_\gamma^r \exp\left\{\left[\lambda_1 + \lambda_2(T - T_0)\right]\bar{\sigma}\right\} \quad (21)$$

$\bar{\sigma} = (\sigma_{11} + \sigma_{22} + \sigma_{33})/3$ is the average stress;

$K$, $A$, r, $\chi_1$, $\chi_2$, $\lambda_1$, $\lambda_2$ are constants of the material.

In most cases this law can be simplified. It allows us to represent, with a fairly good level of accuracy, the behavior of the propellant as a function of various physical parameters: temperature, pressure, and strain rate (Figs 29-32).

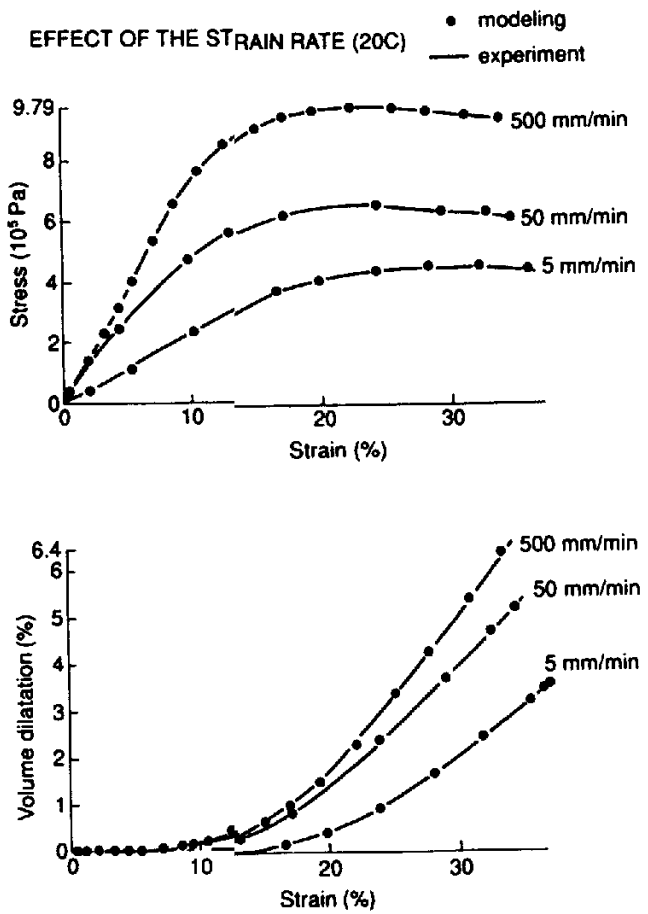


FIG. 6.29. Model of the Farris law behavior.



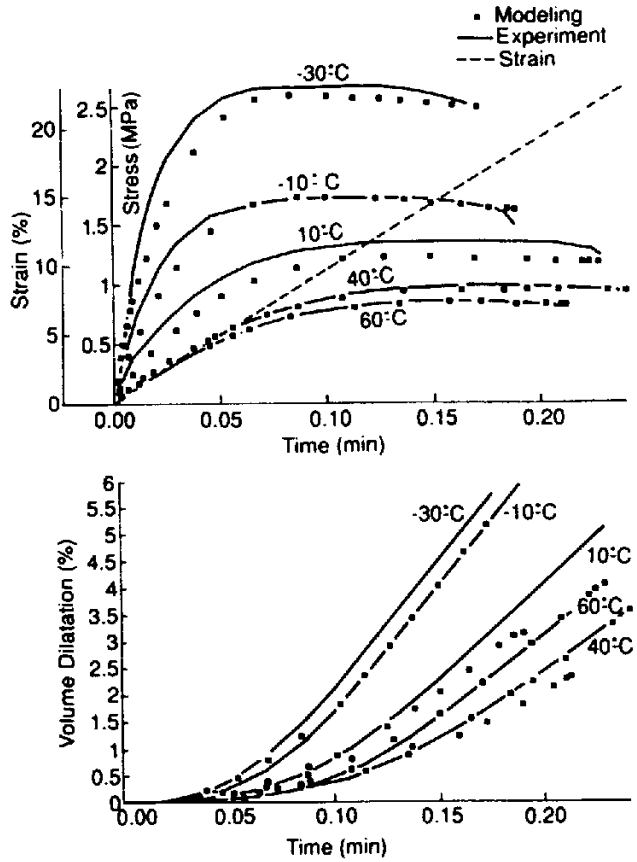


FIG. 6.30. Influence of the temperature.

Some points of the field are modeled with a great lack of precision, which is a serious disadvantage when used systematically. This remark seems to have been justified for most of the models proposed by various authors [13].

In fact, the modeling of a behavior law can be done according to two methods:

(a) Experimental results are written into models according to various mathematical expressions (polynomials, power laws), which are not necessarily supported physically. In this case the precision of the model selected depends on the quantity of tests performed to explore the experimental field.

(b) The choice of a constitutive law to approximate the behavior based upon the modeling of the physical phenomena involved during the tests (for example, with composite propellants, the dissipation of energy

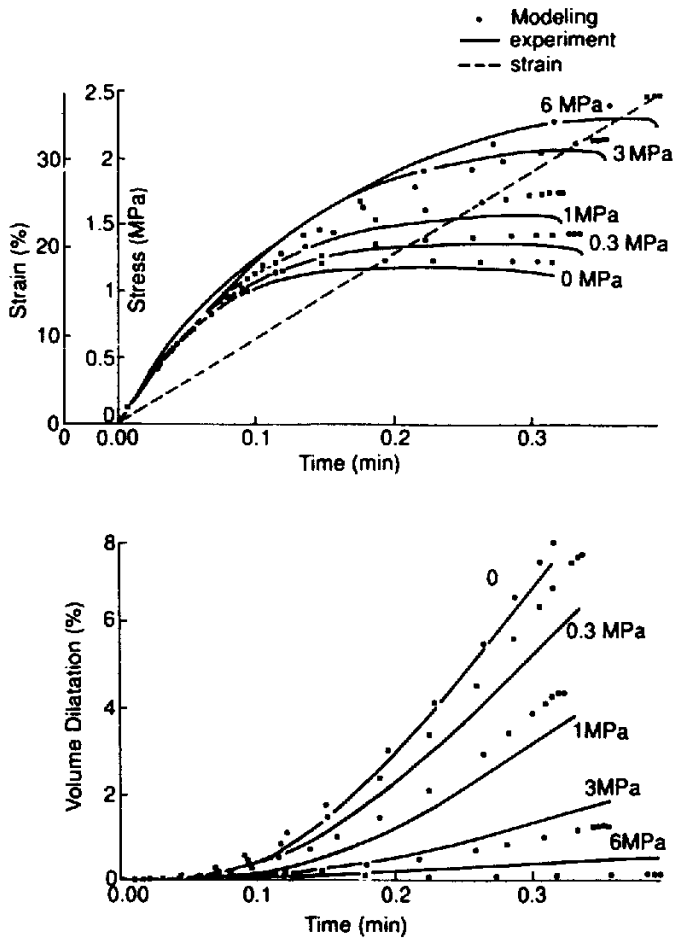


FIG. 6.31. Influence of pressure.

through the creation of vacuum holes, growth of cracks and ripping of the binder until a break occurs). This method, based predominantly on physics, and therefore more real, should allow us to obtain a global modeling of the behavior of propellants, with a good level of accuracy over a fairly extensive experimental field. In fact, the physical phenomena taken into consideration do not correspond to all physical phenomena involved. The simplified assumptions used to create the models do not have the same degree of validity for the whole field examined. For some conditions of utilization, some phenomena that have not been taken into consideration may modify the behavior, and the modeling used will be imprecise.



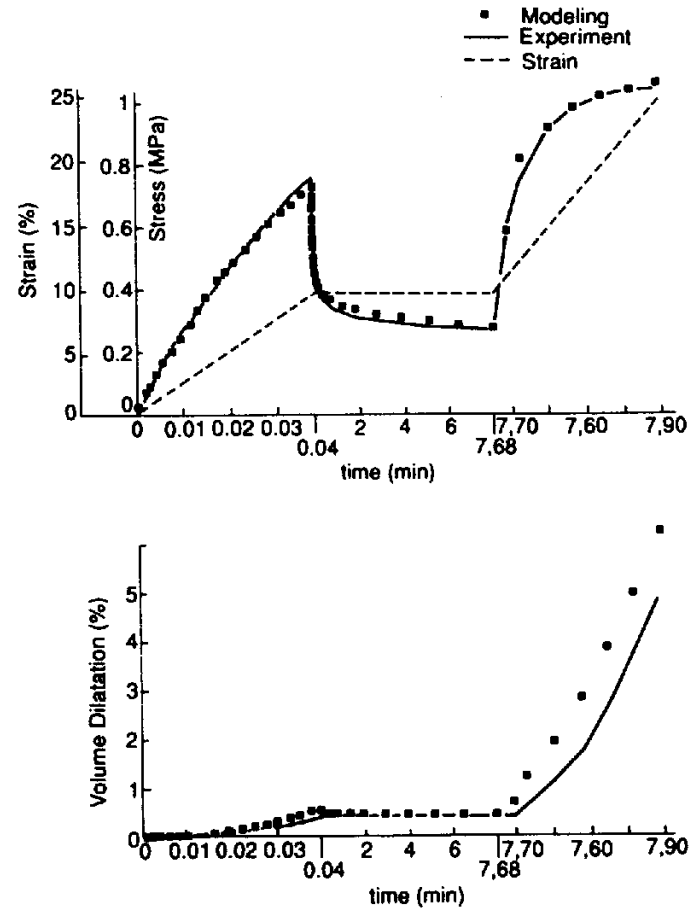


FIG. 6.32. L.R.L. test..

These slightly pessimistic comments do not prevent research activities from continuing, which is a good thing. Even though it seems improbable that we will be able in the short term to use a constitutive law expressing the complex behavior of propellants, the development of modeling, even if it can never be completed, increases considerably our knowledge of propellants and gives us the possibility of improving their structural integrity.

### 4.2.6. *Capability: failure criterion*

#### 4.2.6.1. *Capability* (allowable stress or strain)

The propellant capability is the induced maximum stress or strain necessary to cause failure of the material.

The propellant capability, under tensile load, may be expressed either by the maximum stress $\sigma_m$, or by the corresponding maximum elongation. If cracks appear at elongation $\varepsilon_m$ and propagate throughout the specimen up to $\varepsilon_r$ (Fig. 18), the propellant cannot be used for an elongation ranging between $\varepsilon_m$ and $\varepsilon_r$.

The capability of a propellant is determined experimentally. It is expressed by using master curves (Fig. 33).

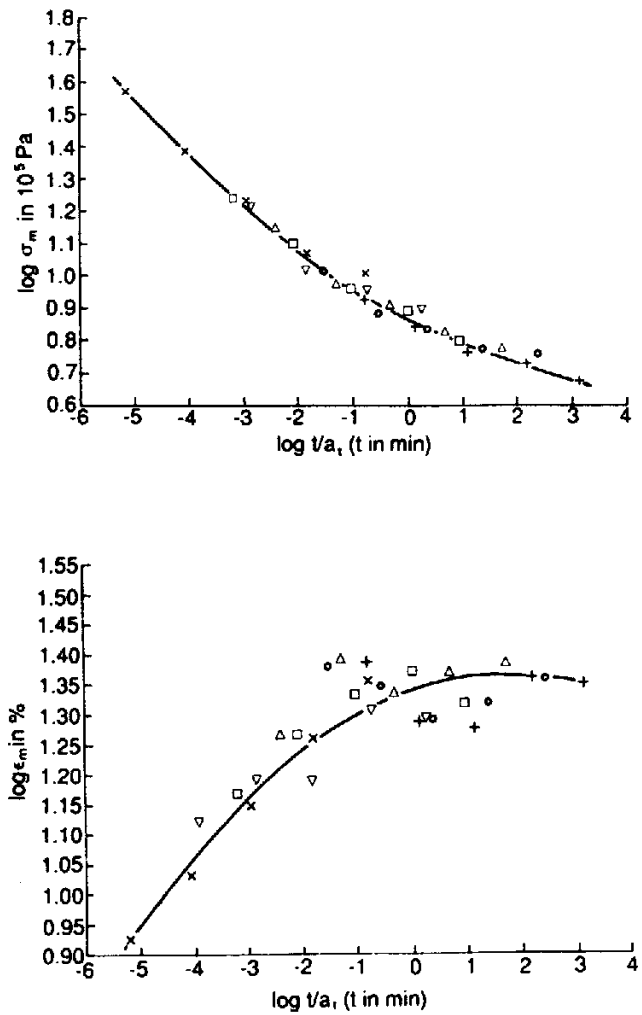


FIG. 6.33. Tensile master curves $\sigma_m$ and $\varepsilon_m$.



### 4.2.6.2. *Failure criterion* [14]

The propellant capability, as defined in Section 4.2.6.1., corresponds to a monodimensional test. The stress tensor is reduced to a single component.

$$\bar{\sigma} = \begin{bmatrix} \sigma_m & 0 & 0 \\ 0 & 0 & 0 \\ 0 & 0 & 0 \end{bmatrix}$$

In a propellant grain the stress tensor has, at each point, more than one non-zero component. Consequently, it is not possible to do a direct comparison between the capability obtained by monodimensional tests and a three-dimensional stress field.

When inducing a mechanical load, there is at each point of the propellant a stress tensor and a strain tensor. These tensors can be characterized by their three principal components and the corresponding invariants (as defined in Section 3). The stress tensor (or strain tensor) for each point of the propellant grain is represented by one point in the principal stress space (or principal strain space). In that space there exists a volume where the propellant keeps its structural integrity, where there is a little damage, and a volume where the propellant is made worthless by significant damage, even possibly a crack. It is sufficient to ensure that the points representative of the stress tensor in the propellant are located in the volume where the propellant keeps its structural integrity.

Generally, the propellant is considered worthless when it is ruptured. The two areas are separated by an assumed continuous surface, called the failure surface. It is defined only in stress, and it is obtained with different tensile tests under different hydrostatic pressures, different temperatures, different tensile rate, and biaxial and triaxial tests.

Several authors have proposed different equations for these surfaces [14]. For propellants in general, it seems that the best-suited equation corresponds to a mixed formula:

- the Stassi formula for the area where the stresses are positive or slightly negative;
- the Von Mises formula for the area where the stresses are negative (Fig. 34).

These two formulae correspond to revolution surfaces centered on the axis $\Delta$ where $\sigma_1 = \sigma_2 = \sigma_3$. Figure 35 shows the intersection of that surface with a plane containing the $\Delta$ axis. Axes $\Delta$ and $Y$ of this new space are related to values using invariants of the stress tensors:

$\Delta$ is the axis of the average stresses $\sigma_{oct} = \frac{1}{3}(\sigma_1 + \sigma_2 + \sigma_3)$ $Y$ is the axis of the octahedral shear stress

$$\tau_{oct} = \tfrac{1}{3}[(\sigma_1 - \sigma_2)^2 + (\sigma_2 - \sigma_3)^2 + (\sigma_3 - \sigma_1)^2]^{1/2}$$

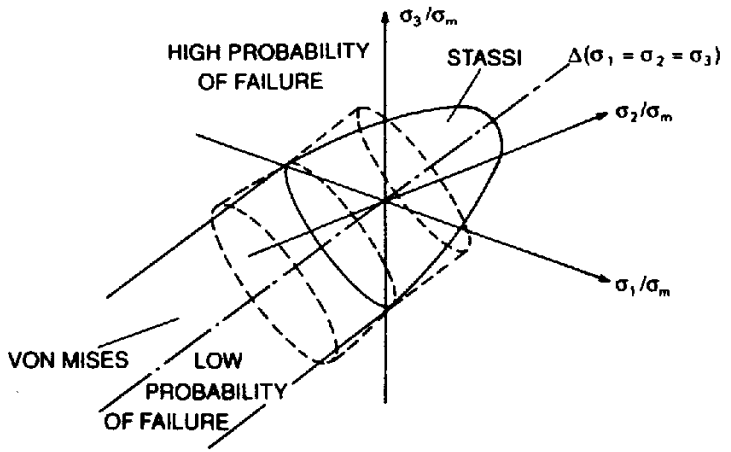


FIG. 6.34. The failure criterion.

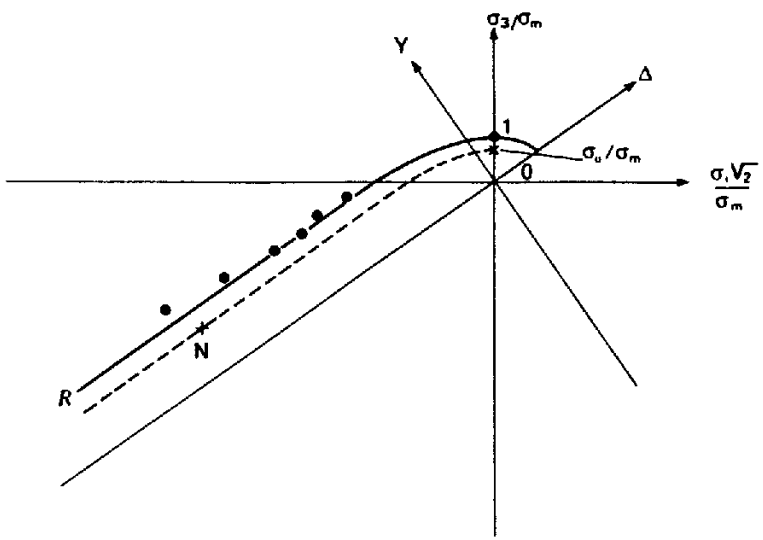


FIG. 6.35. The failure criterion shown in a two-dimensional axis system.

All points representative of the stresses in a propellant grain are located within that plane. Taking a point $M$ in this plane, the homothetic curve to the curve $\mathscr{R}$ (representative of the failure surface) passing through $M$ cuts the axis $\sigma_3/\sigma_m$ at a point whose measurement on this axis is $\sigma_o/\sigma_m$; $\sigma_o$ is called the equivalent stress. It allows us to compare directly the three-dimensional stress state represented by the point $M$ to the maximum stress obtained in a tensile test.



For the Von-Mises part, this equivalent stress is defined by:

$$\sigma_o = [[(\sigma_1 - \sigma_2)^2 + (\sigma_2 - \sigma_3)^2 + (\sigma_3 - \sigma_1)^2]/a]^{1/2}$$

and for the Stassi part:

$$\sigma_o = [(\sigma_1 + \sigma_2 + \sigma_3) + \{(\sigma_1 + \sigma_2 + \sigma_3)^2 + b[(\sigma_1 - \sigma_2)^2 + (\sigma_2 - \sigma_3)^2 + (\sigma_3 - \sigma_1)^2]\}^{1/2}]/c$$

$a$, $b$, and $c$ are coefficients that depend on the material.

*Comment.* The use of this failure criterion implies that the effects of the pressure observed on the stress capability are identical to the effects on the strain capability. It is therefore necessary to verify, experimentally, that the gain contributed by the pressure to the stress is at least equal to the gain contributed to the corresponding strain.

Furthermore, if the failure surface of a propellant is not identical for all stress rates and temperatures tested, the failure criterion defined in this section does not exist. When this occurs, the propellant capability must be determined experimentally under conditions similar to the operating conditions (stress rate, temperature and pressure), using multiaxial specimens.

### 4.2.7. Damage

The capability defined in the preceding section corresponds to an elementary mechanical load, i.e. one rate of load, one temperature and one pressure.

Propellant grains are subjected to various loading conditions whose effects are cumulative in time. It is therefore necessary to introduce the notion of damage, which represents the ability of the material to be subjected to a cumulation of various elementary loads.

Several models have been suggested. Currently, the most widely used model for propellants is the Bills model, based on the Miner model, and defined as follows: [4,23-25]

$$\mathscr{D} = \sum_{i=1}^{N} \frac{t_i}{t_{Ri}} \tag{22}$$

where:

$i$ represents the various elementary loads;
$t_i$ represents the time spent under elementary loads $i$;
$t_{Ri}$ represents the failure time corresponding to the elementary load $i$;
$\mathscr{D}$ is the damage which, by definition, must be less than 1 for the propellant to be used.

When the creep failure curve is written in the form of:

$$\sigma_F \left(\frac{t_R}{a_T}\right)^{1/m} = 1/\mathscr{D}_0 \tag{23}$$

where:

$\sigma_F$ is the applied load in creeping;
$t_R$ is the failure time for applied load $\sigma_F$;
$m$ and $\mathscr{D}_0$ are the coefficients depending on the material.

The damage can be expressed as follows:

$$\mathscr{D}(t) = \mathscr{D}_0\left[\int_0^t (\sigma_e(\tau))^m \frac{d\tau}{a_T}\right]^{1/m} \tag{24}$$

In this manner the entire history of the stress is taken into account, regardless of the nature of the mechanical loads that are applied.

The creep failure curves cannot always be written in the form of eqn (23). In that case, a more general form to express damage is:

$$\mathscr{D}(t) = \mathscr{D}_0(\|\sigma_0\|_m)^{\mathscr{D}_1} + \mathscr{D}_2(\|\sigma_0\|_\infty)^{\mathscr{D}_3} \tag{25}$$

$\mathscr{D}_0$, $\mathscr{D}_1$, $\mathscr{D}_2$, $\mathscr{D}_3$ and $m$ are constants of the material.

### 4.2.8. *Tearing*

Cracks may occur in the propellant as a result of certain manufacturing or handling operations without necessarily compromising the operation of the rocket motor.

To assess the severity of a crack it is necessary to determine the manner in which it propagates itself under the effect of mechanical load.

There are three modes in which a crack propagates itself (Fig. 36).

A stress intensity factor at the tip of the crack is determined for each propagation mode ($K_I$, $K_{II}$, $K_{III}$). It is typically dependent on the initial length $a_0$ of the crack and on the stress that would exist in the area at the bottom of the crack if the crack were not there. As a rule, the propagation rate of cracks obeys a power law for the stress intensity factor.

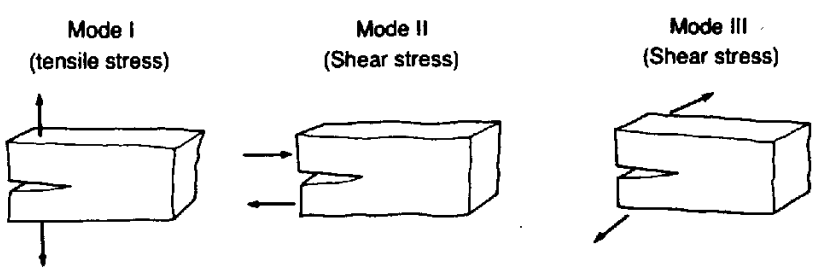


FIG. 6.36. The three modes of propagation of a crack.



Mode I, for example:

$$\frac{da}{dt} = AK_I^n$$

$\frac{da}{dt}$ is the propagation rate of the crack;

$K_I$ the stress intensity factor in Mode I;

$A$ and $n$ constants of the material.

In a propellant grain, when cracks exist, they propagate themselves primarily in Mode I and II.

The tests designed to determine the propagation in Mode I are performed on special specimens (biaxial notched strip specimen) which are subjected to tensile stress in a direction perpendicular to the crack (Fig. 37).

During the test, the length of the crack does not evolve in a continuous manner [26]. But, by proceeding to an integration of the phenomenon, it is possible to obtain an average evolution of the propagation rate of the crack (Fig. 38), as well as the intensity coefficient of the stress.

Crack propagation tests give results that are very scattered. The laws describing the phenomenon can be only an approximation of that phenomenon.

Nonetheless, the law described below [15,16] permits a global representation of the crack propagation phenomenon in propellants (Fig. 39).

$$\frac{da}{dt} = A\frac{K_I^2}{\sigma_m^2 t_m};$$

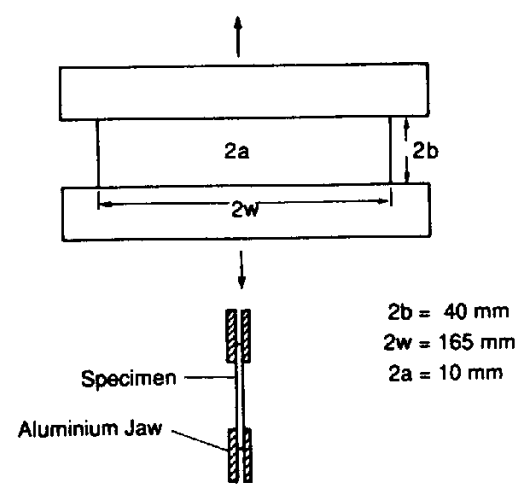


FIG. 6.37. Notched biaxial strip specimen.

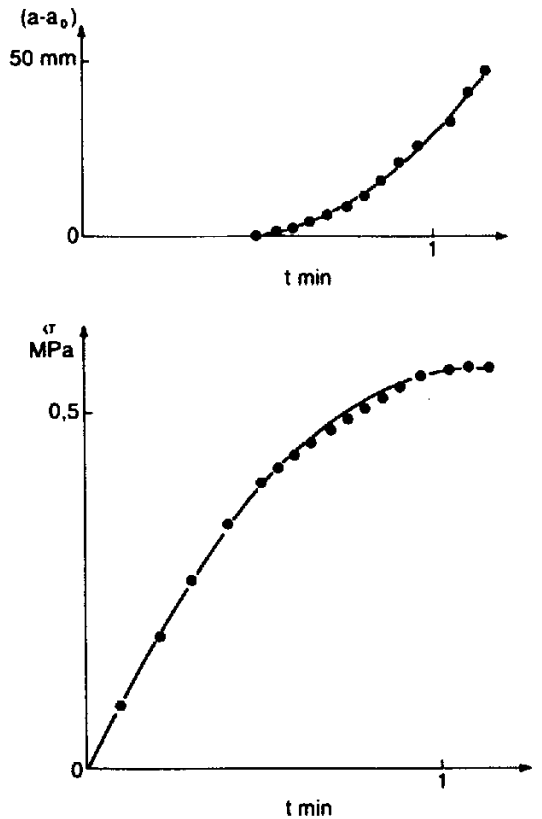


FIG. 6.38. Evolution of the length of a crack and of the stress during a test.

$A$ material constant;

$\frac{da}{dt}$ propagation rate of the crack;

$\sigma_m$ tensile capability of the material for the corresponding mechanical load (same tensile rate);

$t_m$ time to failure corresponding to $\sigma_m$;

$K_I$ stress intensity factor in Mode I.

There are other authors proposing laws for viscoelastic materials [17-19]. A significant amount of research is being done currently in this area; crack modeling in solid propellant grains continues to be done with simple models.



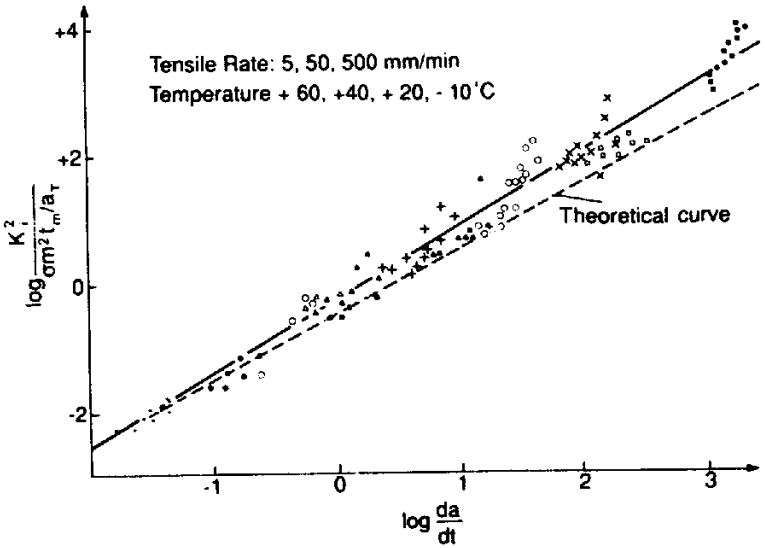


FIG. 6.39. Law of crack propagation.

## 4.3. BONDS (BONDING BETWEEN THE LINER AND THE PROPELLANT)

### *4.3.1. Physical and mechanical nature of the bonds*

The bonds represent physically the adhesion occurring during the propellant curing phase, between the propellant and the liner. This adhesion takes place by the migration through the surface of various products that allow the creation of physicochemical bonds. A detailed analysis of the material in the vicinity of the bonds reveals that there is no bondline, geometrically speaking, but rather a significant gradient of the mechanical properties.

Mechanically, the bonding is represented by a surface separating two homogeneous materials. Consequently, there is a discontinuity of the stress tensor and of the strain tensor through the bondline. From a mechanical point of view there is a continuity of the displacement of all surface points belonging both to the liner and to the propellant, and of the force applied to the surface. All other components are discontinuous.

On the bondline, the force per unit surface is the sum of an elongation component $\sigma_N$, called normal stress, and a sliding component called shear stress (Fig. 40).

$$\vec{F} = \sigma_N \cdot \vec{n} + \tau \vec{t}$$

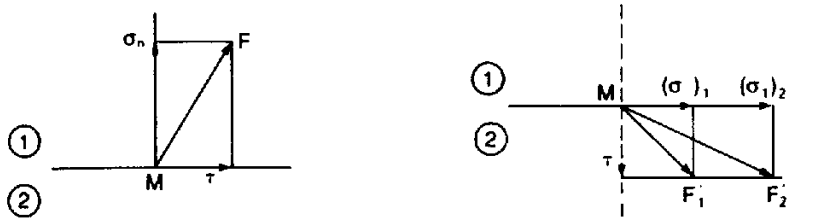


F Applied Force at M relating to bonding plane

$F_1'$ et $F_2'$ Applied Forces at M relating to the plane normal to the bonding plane

At the point M, there are 2 stress tensors

relating to material (1)

$$\begin{bmatrix} \sigma_n & \tau \\ \tau & (\sigma_1)_1 \end{bmatrix}$$

relating to material (2)

$$\begin{bmatrix} \sigma_n & \tau \\ \tau & (\sigma_1)_2 \end{bmatrix}$$

There is continuity of $\sigma_n$ and $\tau$

FIG. 6.40. Discontinuity in the vicinity of a bondline.

The continuity of the force is expressed by the continuity of the normal stress and of the shear stress applied to the bondline. These components are therefore the components that globally characterize the capability of the bonds.

## 4.3.2. *Behavior of the bonds*

### 4.3.2.1. *Micromechanical analysis*

The micromechanical analysis of the behavior of the material in the plane area of the bonding is conducted by taking microspecimens on which the mechanical characteristics under tensile test are determined (Fig. 41). Additional microhardness tests make it possible to confirm the results obtained on the small specimens. There is, in some propellant compositions, an increase in Young's modulus in the vicinity of the bondline, as well as an increase in hardness (Figs 42 and 43).



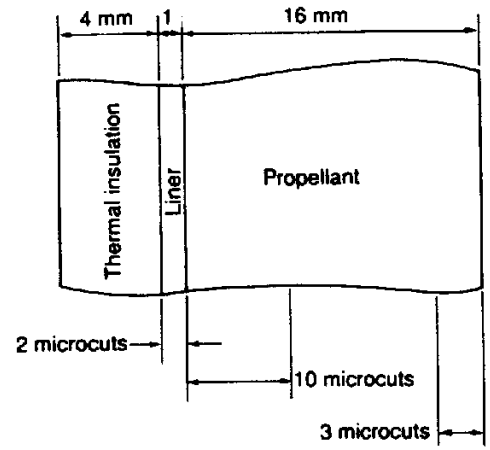


Dimension of the specimens for the micromechanical study
Length = 25 mm Width = 5 mm Thickness = 0,5 mm

FIG. 6.41. Removal of microspecimen in the vicinity of the bondline.

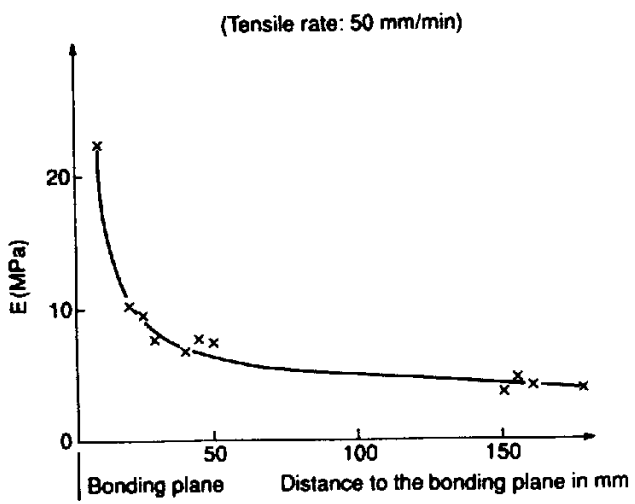


FIG. 6.42. Evolution of the modulus in the vicinity of the bonding plane.

### 4.3.2.2. *Global analysis*

The complex nature of the bonding area having been revealed by the micromechanical analysis, it is therefore possible to mechanically characterize the entire bonding area by assuming that the liner-propellant whole is an

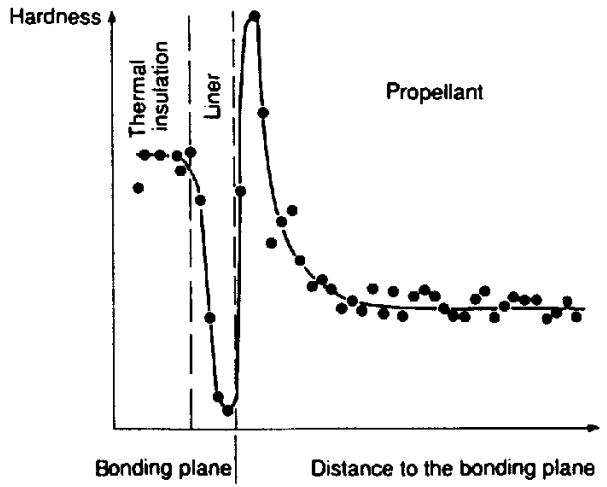


FIG. 6.43. Evolution of the hardness in the vicinity of the bonding plane.

orthotropic material. The symmetry of the superposition of the various materials reduces to five the number of coefficients that need to be determined to characterize the behavior (Fig. 44).

### 4.3.3. *Capability of the bonds*

The capability of the bonds is obtained by applying increasing load until failure of the specimen occurs.

#### 4.3.3.1. *Micromechanical analysis*

This particular analysis, performed on microspecimens described in Section 4.3.2.1, allows us to discover a variation of the maximum stress at break and the corresponding strain in the vicinity of the bonding area (Fig. 45).

#### 4.3.3.2. *Global analysis*

There are two ways of performing the global analysis of the capability:

- by assimilating the bonding area to an orthotropic material;
- by measuring the maximum force applied to the bonding plane.

The first method is simply a prolongation of the method described in Section 4.3.2.2.

The second method consists of measuring the maximum force applied to the bonding plane for different application angles. The specimens used are those described in Fig. 46.



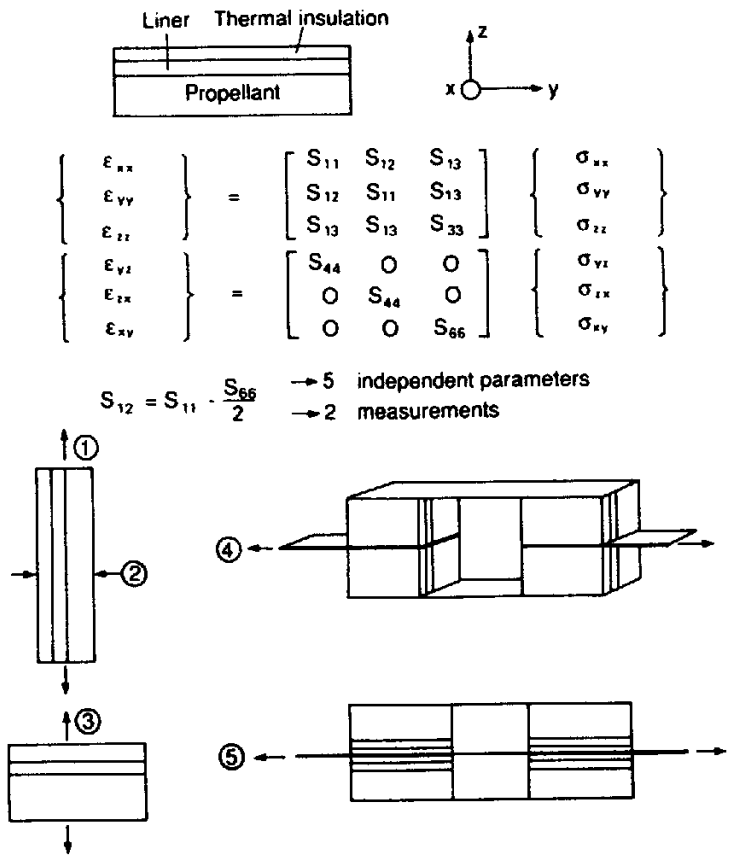


FIG. 6.44. The bonding area is an orthotropic material.

One can identify, in a plane $(\sigma_N, \tau)$ a curve that limits a high probability failure area and a low probability failure area (Fig. 47).

The scattering observed in these tests is important.

In most cases the failure in the propellant occurs in the vicinity of the bonding plane.

The tensile stress specimen used to characterize the bonds (Fig. 46) is not a monodimensional specimen. The maximum stress obtained at the failure of the specimen, in the propellant, in the vicinity of the bonding plane, is lower than the maximum stress obtained on propellant alone from a monodimensional specimen. A tensile test performed on propellant alone with a cubic specimen used for bonding is sufficient to verify the influence of the geometry of the specimen.

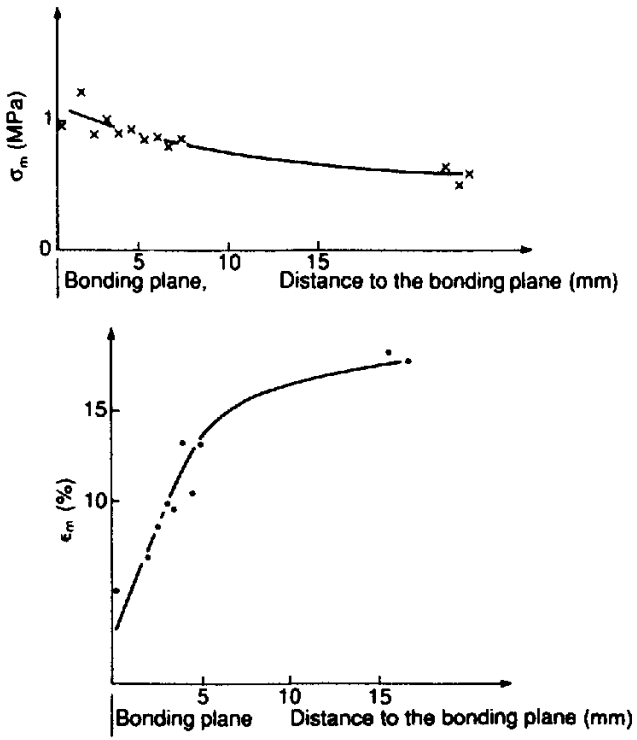


FIG. 6.45. Evolution of $\sigma_m$ and $\varepsilon_m$ in the vicinity of the bonding plane.

### 4.3.4. *Propagation of the debondings; peeling*

The characterization of the ability of an initial debonding to propagate is determined by performing a peeling test. This test is described in Fig. 48. This test is used to categorize, for various liner-propellant assemblies, the force necessary for the debonding to propagate itself, for a given loading rate. The greater the peeling force versus the width of the specimen, the better the structural integrity of the specimen will be, all other things being equal.

As the debonding propagates itself in the propellant, the results of tearing in the corresponding propellant can be used to perform a qualitative correlation.

## 5. Determination of the Induced Stress-Strain (Requirement)

### 5.1. BRIEF BACKGROUND

The determination of the stress existing in a propellant grain subjected to a mechanical load is vital to assess the safety coefficient of this propellant grain.



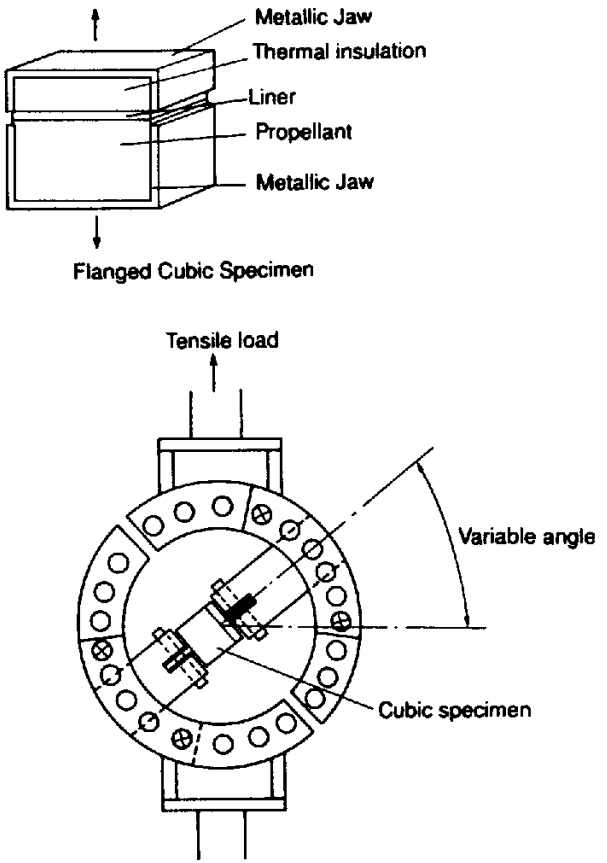


FIG. 6.46. Specimens for bonding tests.

This problem has always been, and continues to be, a constant source of concern. The methods used to resolve it change with the discovery of new technology.

Until the 1960s experimental methods were widely used. Then, with the progress made by numerical methods and computers, numerical analysis became the preferred method. Currently, they are the primary tool, and their use has modified considerably the steps followed to analyze propellant grains. Experimental methods did not allow the analysis of geometries that were too complex. These geometries were the results of the experience — often very extensive — of the designers, but the optimization from the point of view of structural integrity was not always possible (because the experimental methods used were very cumbersome). Computerized methods allow us, on

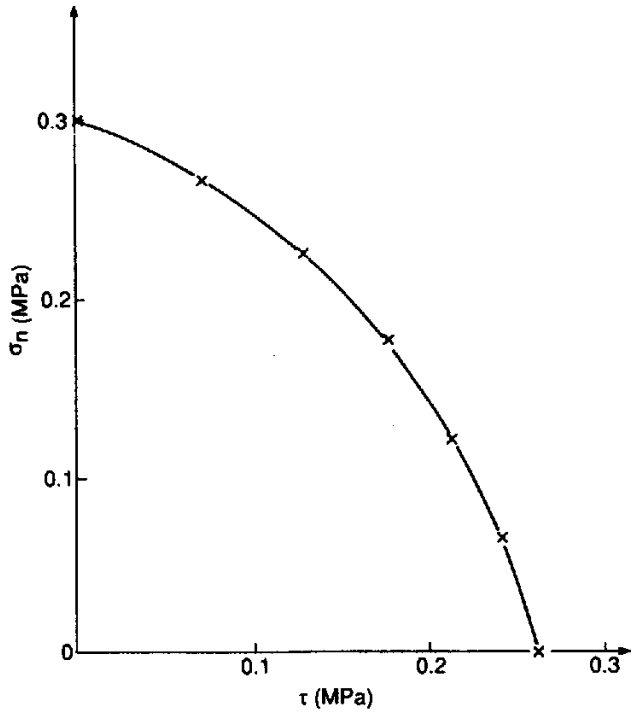


FIG. 6.47. Failure criterion ($\sigma_n$, $\tau$).

the contrary, to analyze a great number of geometries and to select the one geometry that is best suited to solve the problem at hand. The experimental methods are, nevertheless, still used and developed parallel to the computerized methods to validate experimentally the theoretical analyses.

## 5.2. THE EXPERIMENTAL METHODS

When a direct measurement of stress/strain in a propellant grain is used, it usually involves measurements of strains. The analysis of stresses is more difficult because the gages are for the most part larger and can mechanically disturb the environment where they are implanted.

The indirect method most widely used to perform indirect measurements is photoelasticimetry [5]. This allows an experimental determination of the stress. Some transparent materials have the characteristic of becoming birefracting when subjected to a stress field. Polyurethane and some of the epoxy resins have that property. When specimens made of these materials are subjected to a mechanical loading, interference fringes are revealed when the specimens are placed between two polarizing and analyzing filters in the path of a light ray. These fringes are caused by the existence of stresses in the



Sketch of the testing equipment

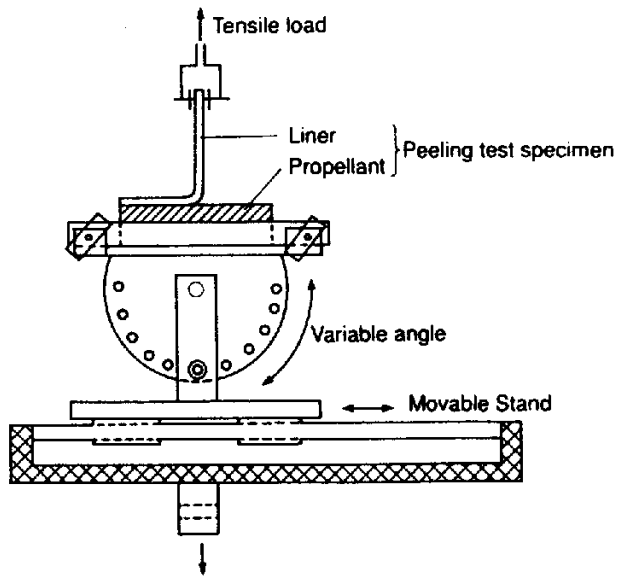


FIG. 6.48. Peeling test.

sample under study. This method consists of preparing samples made of resin shaped like the propellant grain or the portion of the propellant grain under analysis. Reduced scale may possibly be used. A mechanical load is applied to the sample to obtain stresses identical to those present in the propellant grain.

The stress state modifies the optical properties of the sample; these properties are frozen in that particular state by the appropriate thermal cycle. After this, thin slices are cut — they have kept their birefracting state corresponding to the mechanical stress field — and analyzed with a two-dimensional method.

The main difficulties encountered with this method are to obtain the proper geometry and to apply the stress conditions within realistic boundary limits. Moreover, the analysis of the stress field is performed in a material that typically exhibits an incompressible linear elastic behavior.

## 5.3. NUMERICAL METHODS

The subject discussed in this section has been by itself the object of a tremendous number of studies for many years. Today, a significant number of studies continue to be performed. It is therefore not necessary to provide here a detailed description of numerical methods, since there is a large quantity of

good-quality literature on the subject. Their practical use is discussed in Chapter 2. Only special aspects of the structural integrity analysis of propellant grains are listed below.

All mechanical analyses are defined by (Fig. 1):

- a precise description of the geometry to which the mechanical load is applied;
- the boundary conditions depicting the loading conditions;
- the mechanical behavior law of the materials.

The geometry involved in propellant grain is three-dimensional; the mechanical loads applied are static, dynamic, and with or without thermal effects, and the behavior laws are non-linear viscoelastic.

Dealing with the mechanical analysis involves resolving the conservation equations (of the mass, the energy, and the volume for an incompressible material) and the equilibrium equations of the forces and the vectorial moments, taking into account the boundary conditions applied. All of these equations are expressed, in the end, in differential equations for the displacements. The numerical method used is the finite element method. Without going into great details about this method, the subject of an abundant specialized literature ([6] and [7] among many others), the principle may be succinctly described as follows:

The geometry is decomposed into a finite number of small areas (called finite elements) where the function to be determined (the displacement field) is expressed by a function of the coordinates of the points of the areas. This function is usually a polynomial of the first or second degree.

When dealing with propellant grains there is the additional problem of incompressibility. Let us consider the formulation expressed by equations (4)

$$\begin{cases} \sigma'_{ij} = 2G\varepsilon'_{ij} \\ \bar{\sigma} = 3K\bar{\varepsilon} \end{cases}$$

The volume conservation equation (incompressibility assumption) in the case of infinitesimal deformations is expressed by $\bar{\varepsilon} = 0$.

Consequently, the mechanical problem is solvable only to determine the deviatoric tensor, the average stress is indeterminate. There have been a number of methods proposed to determine the average stress. Some iterative methods do not give satisfaction in all cases studied. There is, however, one method particularly well suited for structural analysis of propellant grains. This was developed by Herrmann [20] and consists of assuming the average stress $\bar{\sigma}$ to be an unknown in the problem. There are therefore two types of unknown to determine: displacement unknowns and average stress $\bar{\sigma}$ unknowns.

With the finite element method, the structural analysis is generally performed with linear behaviors of the propellant. The methods that include nonlinear behaviors take an inordinate amount of time for the calculations. In Section 2, however, the description of the mechanical loads imposed on



propellant grains shows that, in the worst conditions (temperature changes and pressurization at firing) and because the propellant is an incompressible material, the strain field in the propellant depends little on the mechanical behavior law. Consequently, the analysis can be performed in the following manner (Fig. 49):

1. calculations are done using the linear and incompressible behavior law to determine the strain field;
2. at the point where the elongation is the greatest, the stress tensor is recalculated, using a behavior law that is more representative for the propellant.

Nowadays, the finite-element computer programs that allow a correct handling of the problems of propellant linear behavior are the programs that have the following characteristics:

- programs dealing with the propellant incompressibility with the Herrmann method;
- types of solid elements:
  - in two-dimensional, elements with eight nodes with the Herrmann formula;
  - in three-dimensional, elements with 20 nodes with Herrmann formula;
  - skin elements to determine stress tensor at free surface.

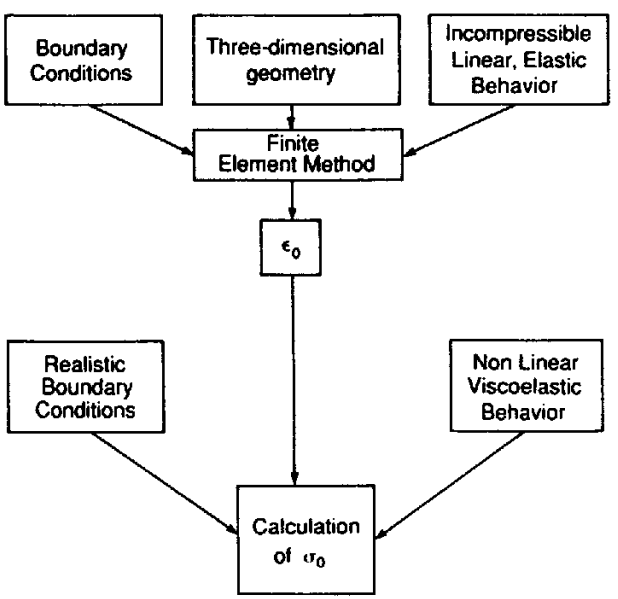


FIG. 6.49. Calculation of the induced load for a non-linear viscoelastic behavior.

The quality of a computer program depends on the structural analysis itself, but also, and most particularly, on the quality of the tools used to prepare and analyze the calculations. These tools are called pre- and post-processors. There is no particular interest in describing these tools here, except for saying that they are extremely useful. They have a great value for a rapid implementation and rational utilization of computer programs for mechanical analysis. The level of professionalism of the designers is often dependent on the quality of these tools.

Figures 50 to 54 provide a summary of the possibilities offered by these analysis methods, without which today's advanced mechanical analysis could not be done.

## 5.4. SIMPLIFIED ANALYTICAL METHODS

For preliminary design analysis, analytical methods are useful when the geometry of the propellant grains can be likened to a specific one-dimensional geometry: the infinite-length hollow cylinder.

The stress/strain and displacements are expressed in a cylindrical coordinates reference system $(r, \theta, z)$. The mechanical state of a cylinder under a specific mechanical load is described by 15 quantities.

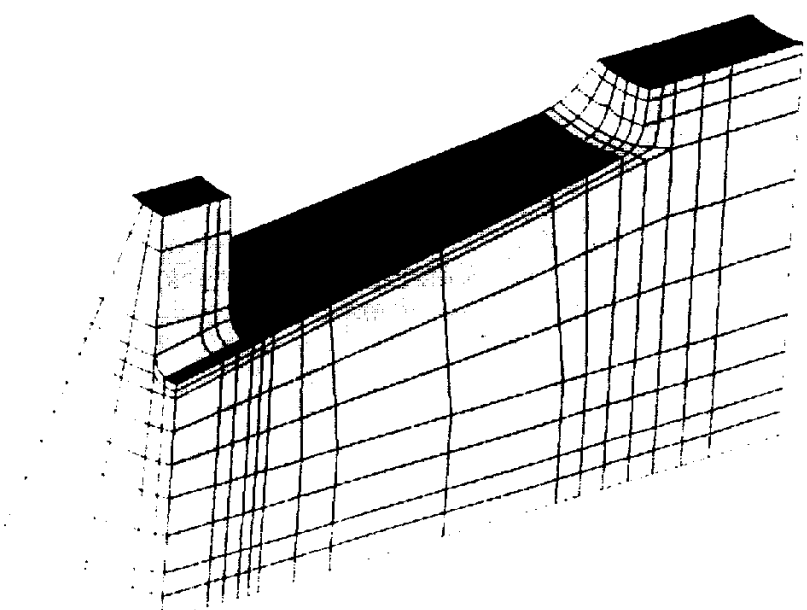

FIG. 6.50. Determination of the induced load. Three-dimensional mesh I.



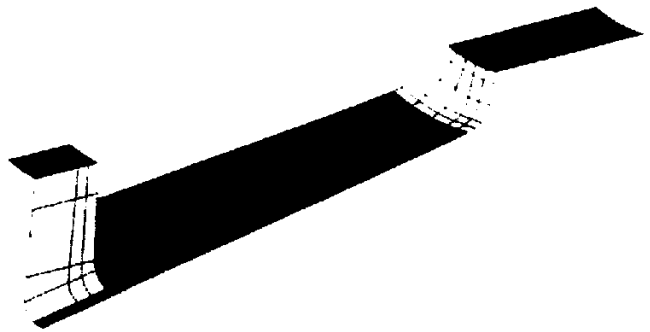

FIG. 6.51. Three-dimensional mesh II. (Skin elements.)

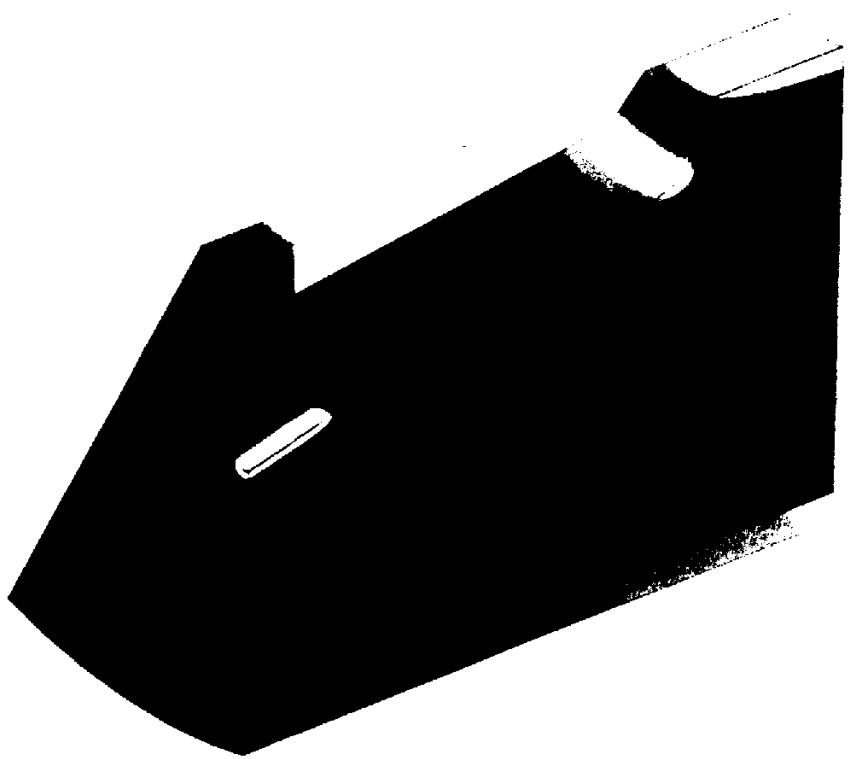

FIG. 6.52. Iso-stresses I. (On skin elements.)

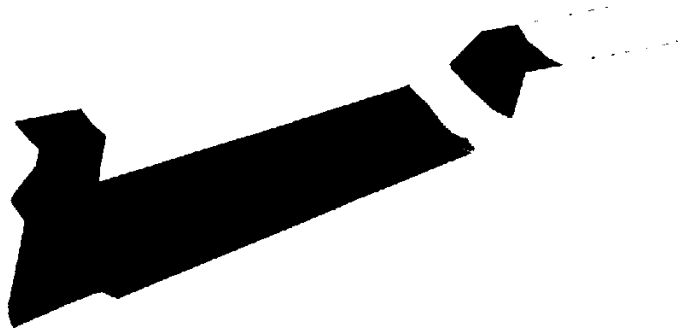

FIG. 6.53. Iso-stresses II. (On a section plane.)

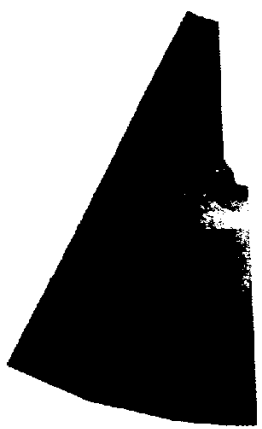

FIG. 6.54. Iso-stresses III.

- six stress components: $\sigma_{rr}$, $\sigma_{\theta\theta}$, $\sigma_{zz}$, $\sigma_{r\theta}$, $\sigma_{rz}$, $\sigma_{\theta z}$
- six strain components: $\varepsilon_{rr}$, $\varepsilon_{\theta\theta}$, $\varepsilon_{zz}$, $\varepsilon_{r\theta}$, $\varepsilon_{rz}$, $\varepsilon_{\theta z}$
- three displacement components: $u_r$, $u_\theta$, $u_z$

In an infinite-length cylinder, the displacement at each point is expressed by only one component $u_r$; it is a plane strain assumption:

$$u_\theta = 0, u_z = 0 \text{ and } u_r = u_r(r)$$

$$\Rightarrow \varepsilon_z = 0, \varepsilon_r = \frac{\partial u_r}{\partial r}, \varepsilon_\theta = \frac{u_r}{r}$$

and for axisymmetric boundary conditions:

$$\varepsilon_{r\theta} = \varepsilon_{\theta z} = \varepsilon_{rz} = 0$$

$$\sigma_{r\theta} = \sigma_{\theta z} = \sigma_{rz} = 0$$



When the material is assumed to be incompressible, Hooke's thermoelastic law is written as:

$$\varepsilon_{rr} = \frac{3}{4E}(\sigma_{rr} - \sigma_{\theta\theta}) + \frac{3}{2}\alpha\Delta T \tag{26}$$

$$\varepsilon_{\theta\theta} = \frac{3}{4E}(\sigma_{\theta\theta} - \sigma_{rr}) + \frac{3}{2}\alpha\Delta T$$

where:

$E$ = Young's modulus;

$\alpha$ = linear thermal expansion coefficient of the material;

$\Delta T = T - T_0$;

$T$ = temperature at which the stress occurs;

$T_0$ = equilibrium temperature (at which stress is zero).

The equation of equilibrium is written:

$$\frac{\partial \sigma_{rr}}{\partial r} = \frac{\sigma_{\theta\theta} - \sigma_{rr}}{r} \tag{27}$$

and the strain-displacement relation

$$\frac{\partial \varepsilon_{\theta\theta}}{\partial r} = \frac{\varepsilon_{rr} - \varepsilon_{\theta\theta}}{r} \tag{28}$$

From eqns (26), (27) and (28), we can write:

$$\frac{3}{4E}\frac{\partial(\sigma_{\theta\theta} - \sigma_{rr})}{\partial r} + (\sigma_{\theta\theta} - \sigma_{rr})\left[\frac{3}{4}E\frac{\partial(1/E)}{\partial r} + \frac{3}{2E}\frac{1}{r}\right] + \frac{3}{2}E\frac{\partial \alpha\Delta T}{\partial r} = 0 \tag{29}$$

For a hollow circular cylinder with
$a$: inside radius
$b$: outside radius
the general solution is written:

$$\sigma_{rr}(r) = \int_a^r -\frac{2E}{r^3}F(r)dr + F(a)\int_a^r -\frac{2E}{r^3}dr + \zeta_1\int_a^r \frac{E}{r^3}dr + \zeta_2 \tag{30}$$

$$\sigma_{\theta\theta}(r) = -\frac{2E}{r^2}\int_a^r r^2\frac{\partial \alpha\Delta T}{\partial r}dr + \zeta_1\frac{E}{r^2} + \sigma_{rr}(r) \tag{31}$$

$\zeta_1$ and $\zeta_2$ are integration constants determined by the boundary conditions. $F(r)$ is the primitive of $r^2$ $(\partial\alpha\Delta T/\partial r)$.

When the temperature is uniform and the modulus constant in the entire geometry, the general solution will be:

$$\sigma_{rr}(r) = C_1 - \frac{C_2}{r^2} \tag{32}$$

$$\sigma_{\theta\theta}(r) = C_1 + \frac{C_2}{r^2} \tag{33}$$

$C_1$ and $C_2$ are determined by the boundary conditions.

### 5.4.1. *Uniform thermal shrinkage in a case-bonded cylinder*

When the propellant is bonded to an non-deformable, rigid motor case, with a very small linear thermal expansion coefficient when compared to that of the propellant, the boundary conditions will be expressed by:

$\sigma_{rr}(a) = 0$, because the inside surface of the cylinder is a free surface;
$u_r(b) = 0$, $\varepsilon_{\theta\theta}(b) = 0$, because there is no displacement of the propellant points bonded to the case.

Consequently:

$$\begin{cases} \sigma_{rr}(r) = E\dfrac{b^2}{a^2}\alpha\Delta T\left(1 - \dfrac{a^2}{r^2}\right) \\ \sigma_{\theta\theta}(r) = E\dfrac{b^2}{a^2}\alpha\Delta T\left(1 + \dfrac{a^2}{r^2}\right) \\ \varepsilon_{\theta\theta}(r) = -\dfrac{3}{2}\alpha\Delta T\left(\dfrac{b^2}{r^2} - 1\right) \end{cases} \tag{34}$$

- The circumferential strain $\varepsilon_{\theta\theta}$ is maximum in the central port at $r = a$.

$$\varepsilon_{\theta\theta}(a) = -\frac{3}{2}\alpha\Delta T\left(\frac{b^2}{a^2} - 1\right)$$

- The normal stress $\sigma_{rr}$ is maximum at the propellant/case bonding at $r = b$.

$$\sigma_{rr}(b) = -E\alpha\Delta T\left(\frac{b^2}{a^2} - 1\right)$$

With this type of geometry and a mechanical load corresponding to a uniform thermal shrinkage, strains are independent of the propellant Young's modulus and stresses are directly proportional to that modulus. Stress at the free surface and at the bonding, in addition, is dependent on $b^2/a^2$. The volumetric loading fraction expressed by the ratio $b^2/a^2$, will have an important effect on the stress.



Propellant grains have a finite length. There are corrective factors [27] allowing the determination of the stress tensor in a finite-length circular cylinder. These factors are given in diagrams (Parr diagrams).

All stresses/strains for this type of mechanical load are proportional to the $\alpha\Delta T$ product. That is why $\alpha$, the linear thermal expansion coefficient of the propellant, must be well determined.

### 5.4.2. *Internal pressure* p *on a case-bonded cylinder*

When the motor case in which the propellant grain is located is a thin one, the boundary conditions are written as:

$$\alpha\Delta T = 0$$
$$\sigma_{rr}(a) = -p$$
$$\varepsilon_{\theta\theta}(b) = -k\sigma_{rr}(b)$$

where $k$ is the flexibility coefficient of the case

$$k = \frac{(1 - \nu_c^2)b}{E_c \cdot h}$$

$\nu_c$ = Poisson's ratio of the motor case;
$E_c$ = Young's modulus of the motor case;
$h$ = thickness of the motor case.

For a motor case showing little deformation ($k$ is very small), simplifications allow us to obtain:

$$\begin{cases} \varepsilon_{\theta\theta}(r) = -\varepsilon_{rr}(r) = kp\dfrac{b^2}{r^2} \\ \sigma_{rr}(r) = \dfrac{2}{3}kpE\left(\dfrac{b^2}{a^2} - \dfrac{b^2}{r^2}\right) - p \\ \sigma_{\theta\theta}(r) = \dfrac{2}{3}kpE\left(\dfrac{b^2}{a^2} + \dfrac{b^2}{r^2}\right) - p \end{cases} \tag{35}$$

As with the thermal load, strains are independent of the propellant Young's modulus, and stresses are proportional to that modulus. The loading ratio, when it grows, increases the level of the stresses in the propellant. Finally, the induced stress/strain depends greatly on the flexibility coefficient of the motor case. The smaller the flexibility coefficient, and consequently the higher the Young's modulus of the motor case, the lower the induced stress/strain will be.

## 5.5. COMMENTS ON THE NECESSITY OF INCOMPRESSIBLE ANALYSES

The mechanical analysis of incompressible materials involves a discontinuity which is expressed with a special formula. A material is considered incompressible when it sustains a deformation while maintaining its constant volume under the effect of applied mechanical load. Based on this definition, the particularity of the incompressibility characteristic does not seem evident. But a deformation under constant volume implies that the material has been provided with a shape that allows such a deformation. The amount of free surface has a determining impact on the rigidity of the object. For example: a viscous liquid has no rigidity; a flexible polyethylene bottle has a low rigidity when it is empty. When that same bottle is completely filled with viscous liquid, the combination exhibits a rigidity under pressure that allows an integral transmission of loads. This is the basic principle which allows hydraulic systems to transmit significant energy quantities.

Incompressible materials are, therefore, sensitive to confinement, which can be defined by the ratio of the volume of the object versus the surfaces free to sustain deformation. An infinite confinement corresponds to an infinite rigidity of the object. This is the meaning of the discontinuity mentioned at the beginning of this section.

- What is the effect of incompressible behavior on the equations?

Based on eqns (1) and (4), assuming infinitesimal deformations, constant volume deformations imply the following relation:

$$\frac{\Delta V}{V_0} = \sum_{i=1}^{3} \varepsilon_{ii} = 0$$

which, in terms of the behavior parameters, is expressed by:

$$\nu = 0.5 \text{ or } K \to \infty \text{ as } \frac{G}{K} \to 0$$

therefore the stress deviator is determined directly by the existing strain field, but the average stress is mathematically undeterminate.

$$\bar{\sigma} = Ke \text{ with } K \underset{e=0}{\to} \infty$$

This average stress is determined physically by the geometry and the confinement.

- In fact, the measurement of the bulk modulus of a propellant gives a finite value; this value is very high in comparison with the value of the shear modulus. It is that significant difference between the compressibility modulus and the shear modulus that confers the incompressible property to propellants.
- What is the behavior of a propellant in the shape of a grain?



Consideration of the incompressibility is of concern only with case-bonded propellant grains. Typically, this type of propellant grain has a higher volumetric loading fraction. All of the propellant surfaces are bonded to the motor case; the only free surfaces are those in the combustion chamber. The higher the volumetric loading fraction, the greater the confinement of the propellant will be.

In general, stresses induced by thermal shrinkage and by pressure rise at the beginning of firing are the most severe.

The average level of strain is often lower than the strain at which vacuum holes occur (i.e. at which the propellant becomes compressible).

Only a small volume of the propellant has a significant strain level, making it compressible. This low volume of compressible propellant (with vacuum holes) does not modify the incompressible behavior of the major portion of the propellant. Simple calculations (Fig. 55) show that because the volume of propellant with vacuum holes is low, the maximum induced stress/strain can be determined by assuming that the entire propellant is incompressible. This is particularly applicable to the stress/strain induced by thermal shrinkage; at the time of firing, the behavior of propellant under pressure likens it to an incompressible material, whatever the level of applied load.

It is therefore necessary to take into account the incompressible nature of the propellant to evaluate induced stress/strain in case-bonded grains, and it is the determination of average stress at each point which allows an accurate mechanical analysis. The average stress is not dependent on the propellant behavior, and a mechanical analysis taking into consideration the incompressible elastic linear behavior of the propellant is sufficient. The viscoelastic properties may be introduced to calculate the stress deviators.

Some calculations based on a simple geometry allow us to summarize the importance of incompressibility.

The geometry used is an infinite length cylinder with an inner diameter of 100 mm and an outer diameter of 400 mm. A temperature change of $-100°C$ is induced. The external surface of the cylinder is bonded to a rigid, nondeformable case. The calculations are done with a finite element program including Herrmann's formulation to treat incompressible behavior. This program also includes classic elements, allowing it to process compressible materials. In addition, the elements with the Herrmann formula allow the processing of materials with any Poisson's ratio, including $\nu = 0.5$.

*First analysis.* The impact of Poisson's ratio on the infinite-length cylinder is indicated in Fig. 56.

The induced stress is represented by an equivalent stress (Stassi stress), which takes the average stress into account; it is at a maximum on the free surface and is heavily dependent on the value of Poisson's ratio (Fig. 57).

*Second analysis.* The propellant is considered to be very compressible (Poisson's ratio equal to 0.33), and the analysis is done with two types of element: the classic element and the Herrmann formula element. The results,

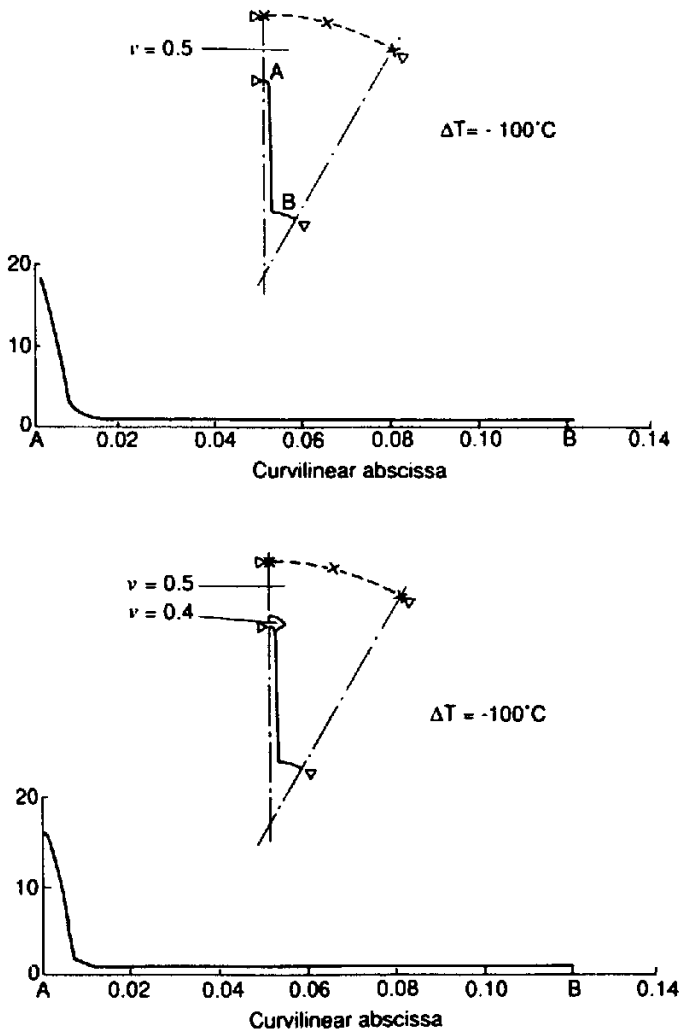


FIG. 6.55. Calculation without and with compressible volume. (Plane strain assumption.)

when compared to the analytical solution, reveal a high level of correspondence between the numerical analysis and the analytical solution (Fig. 58).

*Third analysis.* Finally, a third analysis is performed, for propellants exhibiting a low compressibility ($\nu = 0.495$).

A low-compressibility element can be analyzed with a classic element. The results listed in Fig. 59 show good agreement between the analytical solution



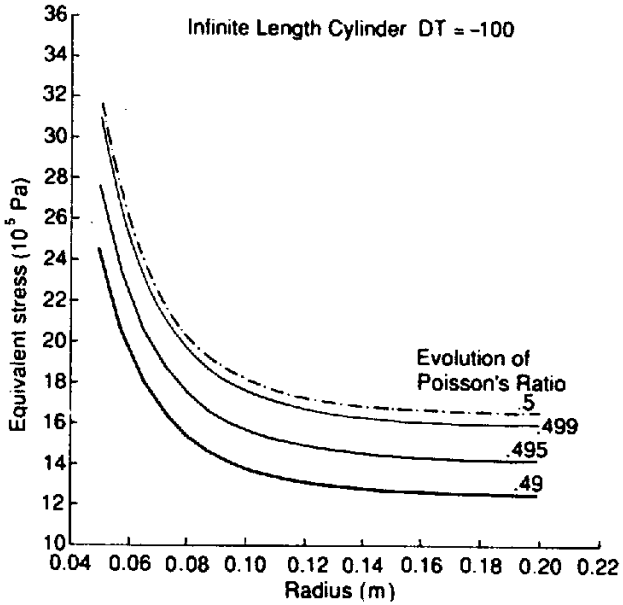


FIG. 6.56. Influence of Poisson's ratio on the equivalent stress.

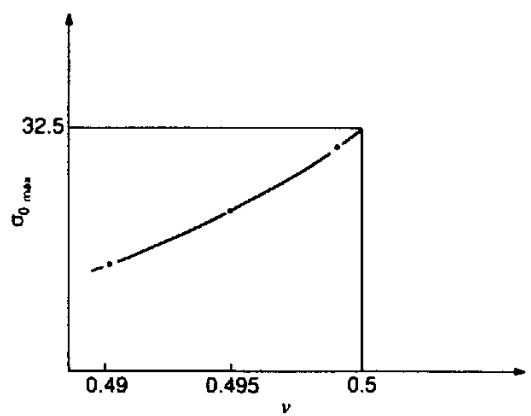


FIG. 6.57. Influence of Poisson's ratio on the equivalent stress on the free surface.

and the analysis done with the Herrmann's formulation. Results obtained with the classic elements are completely erroneous.

The Von-Mises stress, which depends solely on the stress deviators and not at all on the average stress, is analyzed with two types of elements:

- the classical element formulated in displacement;
- the Herrmann formula element.

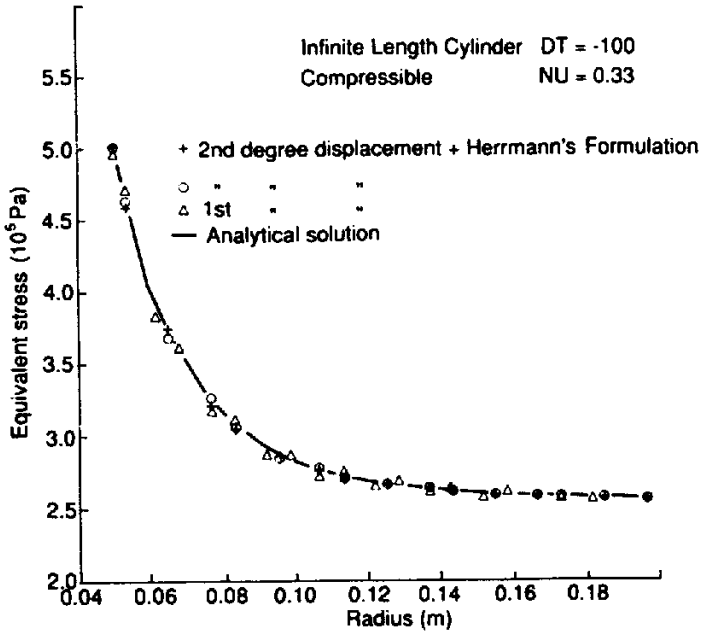


FIG. 6.58. Comparison of Herrmann's formulation and classical formulation applied to a compressible material.

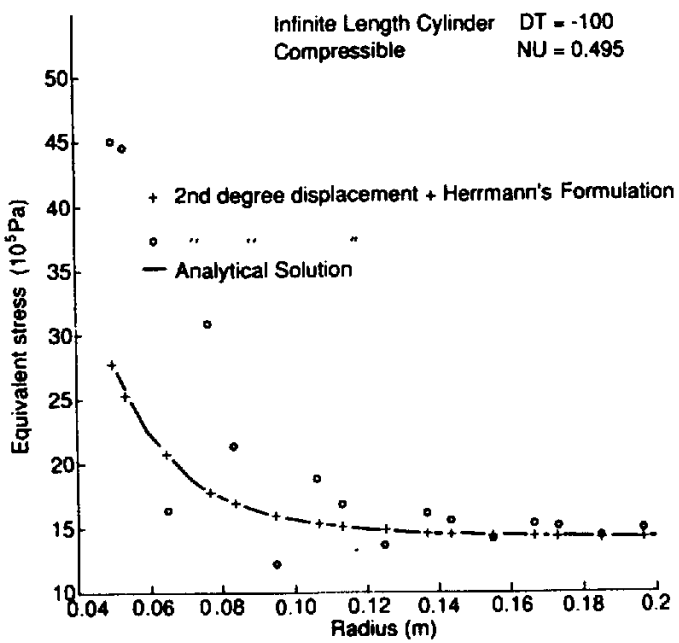


FIG. 6.59. Comparison between Hermann's formulation and classical formulation applied to a quasi incompressible material.



The good agreement between both numerical analysis and analytical solution (Fig. 60) demonstrates that correctly solving an incompressible problem consists in determining the average stress at each point.

## 6. Determination of the Factor of Safety

Following the description in the preceding sections of the methods used to determine the capability and the induced stress/strain, the next logical step is the determination of the structural factor of safety:

$$K = \frac{C}{S}$$

In fact, the problem is really complex, because a propellant grain is subjected to very varied mechanical loads, and the cumulation of the corresponding induced stress/strain complicates the determination of a factor of safety. The capability of the propellant of a case-bonded grain which experiences temperature changes from 50°C to 20°C in a few days, which is then subjected to the force of gravity over a period of several months, and which finally is subjected at the time of firing to a pressure rise in a few milliseconds, is difficult to determine.

With a cumulation of mechanical stresses, the difficulty resides in the definition of the capability that should be taken into consideration. The

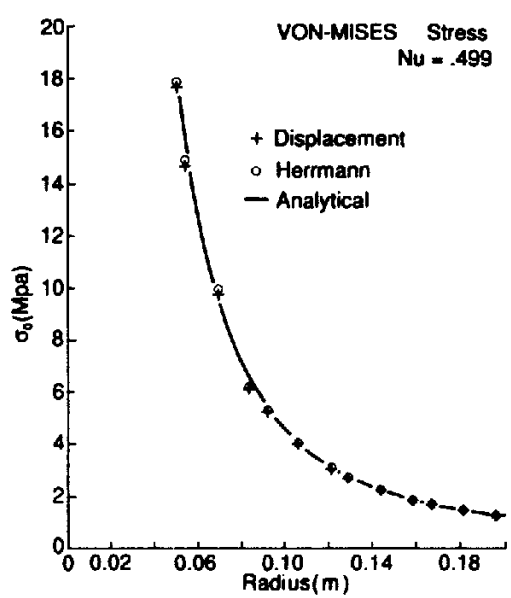


FIG. 6.60. Comparison of the deviatoric stresses obtained by the Herrmann's formulation and the classical formulation in a quasi incompressible material.

induced stresses strains can be combined using the classic additivity laws (making sure that the components of the stress and strain tensors are added only when they are expressed in the same coordinates system).

One method used to assess the capability resulting from the cumulation of mechanical loads consists in submitting a propellant specimen to a succession of mechanical loads experienced by the propellant, under identical temperature, pressure, and loading rates. This highly experimental method does not always permit the determination of real operation conditions of a propellant, because it would require the use of very heavy and costly test facilities. A low-speed tensile stress, for example, applied while simultaneously varying the temperature, and followed by a rapid and progressive increase of pressure from 1 to 10 MPa, is not a simple operation to carry out!

Another method consists of defining the factor of safety of each of the basic mechanical loads, such as temperature changes, the force of gravity, the pressure rise at firing, and others, after which the resulting factor of safety will be a function of each basic factor of safety. Nevertheless, whatever the method used, the factor of safety calculated from stresses or strains must be equal to 1 at grain rupture and, similarly, the reliability calculated using each of the methods must be identical. It is therefore of prime importance to verify each of the methods on reduced-size objects subjected to various mechanical loads leading to failure.

The methods used to calculate the factors of safety are described below. Tests are performed on simple geometries to compare these methods, and eventually improve them. They are described at the end of this section.

## 6.1. FACTOR OF SAFETY OF PROPELLANT GRAINS

### 6.1.1. *Factor of safety in cumulative damage theory*

Damage, described in Section 4.2.7, characterizes the damage done to propellant during its useful life. By definition, it varies over time from 0 to 1:

$\mathscr{D}(0) = 0$ Corresponds to sound propellant grain after its manufacture:
$\mathscr{D}(t_R) = 1$ Corresponds to the failure of the propellant (failure time $t_R$).

The factor of safety is simply deduced from damage $\mathscr{D}(t)$ using the relation

$$K_{\mathscr{D}}(t) = \frac{1}{\mathscr{D}(t)} \tag{36}$$

Defined in that manner, the factor of safety varies over time from infinity to 1



In Section 4.2.7 an expression was suggested for the damage from experimental results obtained from creeping tests (eqn 24):

$$\mathscr{D}(t) = \mathscr{D}_0\left(\int_0^t [\sigma_e(\tau)]^m d\tau\right)^{1/m}$$

This equation calls for several remarks:

*Remark 1.* The factor of safety defined from eqn (24) is written:

$$K_{\mathscr{D}}(t) = \frac{1}{\mathscr{D}_0} \times \frac{1}{\left(\int_0^t [\sigma_e(\tau)]^n d\tau\right)^{1/m}} \tag{37}$$

In this relation: $1/\mathscr{D}_0$ represents the capability of the propellant; it is an experimental datum.

$$\left(\int_0^t [\sigma_e(\tau)]^m d\tau\right)^{1/m}$$

stands for the induced stress in the propellant grain; it is a value obtained by calculations.

$K_{\mathscr{D}}$ is, in fact, the ratio of a capability to an induced stress.

*Remark 2.* Equation (24), providing a damage type, can also be written in the following manner:

$$[\mathscr{D}(t)]^m = D(t) = \mathscr{D}_0^m \int_0^t [\sigma_e(\tau)]^m d\tau \tag{38}$$

$D(t)$ varies from 0 to 1, and therefore corresponds to another expression of the damage that has the same definition.

In fact, eqn (38) is the equation that corresponds to the initial definition of the damage, and best expresses the physical phenomenon. For example, in a tensile test during which the stress varies in a linear fashion over time, the two types of damage are written:

$$\mathscr{D}(t) = \mathscr{D}_0 \dot{\sigma}_0 \left(\frac{1}{m+1}\right)^{1/m} t^{m+1/m}$$

$$D(t) = \mathscr{D}_0^m \dot{\sigma}_0^m \frac{1}{m+1} t^{m+1}$$

The plotting of these two forms of expression is given in Fig. 61 for a realistic value of parameter $m(m = 10)D(t)$, representing a linear cumulation of the damage, and demonstrates the fact that the damage sustained by the propellant is very low up to a fairly high value of the stress, relative to the maximum stress $\sigma_m$.

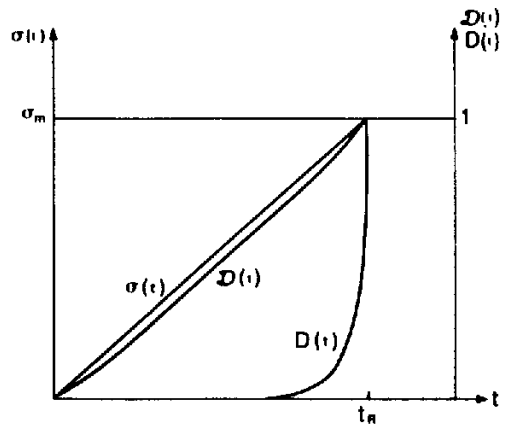


FIG. 6.61. Damage for a linear evolution of the stress.

For example, if the propellant is to be subjected to stress cycles, illustrated in Fig. 62, during which the stress varies between 0 and $\alpha_m$, where $\sigma_m$ is the maximum stress for the tensile test at the same stress rate, and $\alpha$ the coefficient ranges from 0 to 1, the number of cycles $N$ it can withstand is dependent on the value of the coefficient $\alpha$ and is given, based on eqns (24) or (38), by:

$$N = \left(\frac{1}{\alpha}\right)^{m+1}.$$

With a realistic value for $m(m = 10)$, the values obtained are indicated in Table 2.

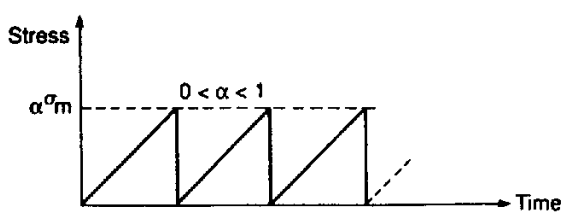


FIG. 6.62. Stress cycles imposed on a specimen.

TABLE 2

| α | Number of cyles |
|---|---|
| 0.5 | 2048 |
| 0.8 | ~11 |
| 0.9 | ~3 |



Under these conditions the damage sustained by the propellant for a 0.5 $\sigma_m$ cycle is negligible in comparison with the damage sustained at a 0.9 $\sigma_m$ cycle.

*Remark 3.* Strain damage can be defined based on experimental results obtained from relaxation tests, for various strains, up to failure. Typically, the formula is very close to that given by eqn (24) but the value of exponent $m$ is greater ($m > 30$).

Similarly, the factor of safety is given by the inverse of the damage.

*Remark 4.* The cumulation of induced stresses/strains presents no problem when the factor of safety is calculated in terms of damage, because the induced stress/strain is integrated over time, and the capability, represented by $1/\mathcal{D}_0$, is representative of multiple tests performed under very varied conditions. The use of the factor of safety in terms of damage seems, therefore, to resolve all cumulation problems. Although it is certainly the factor that deals best with the problem, it should not be forgotten that eqn (24) is a simple equation applied only when the creep failure curve is a straight line ($\log \sigma_F = A \log t_R + B$). In propellants, the equations expressing the damage are usually more complex (eqn 25) and, in any case, they must be experimentally determined and verified for each propellant.

### 6.1.2. *Factor of safety defined with strains*

For an elementary mechanical load, this is defined by:

$$K_\varepsilon = \frac{\varepsilon_m}{\varepsilon_0} \tag{39}$$

where:

$\varepsilon_m$ = strain under tensile stress relative to the maximum stress, for the parameters of loading rate and temperature corresponding to the applied mechanical load;

$\varepsilon_0$ = strain corresponding to the point where the induced strain is maximum; it is determined from the equivalent stress, assessed with the failure criterion, for a Young's modulus $E$ that corresponds to parameters of loading rate and temperature of the mechanical load:

$$\varepsilon_0 = \frac{\sigma_0}{E}$$

This definition of equivalent strain implies that the multidimensional effects are the same for stresses as for strains. In particular, the effect of pressure must be identical for the stress capability as for the strain capability (see Section 4.2.4.).

One method for the cumulation of basic factors of safety determined for strain is obtained from remarks 2 and 3 of the preceding section. When $m$ is

very large ($1/m$ close to 0), the initial definition of damage can no longer be used because, during a relaxation test, the failure time tends to be infinite.

Damage, in this situation, is written in other forms, including:

$$\mathcal{D} = \max\left(\frac{\varepsilon_{oi}}{\varepsilon_{mi}}\right) \tag{40}$$

where:

$\varepsilon_{oi}$ = equivalent strain sustained by the propellant grain for an elementary mechanical load $i$;
$\varepsilon_{mi}$ = strain at failure of the propellant grain for the elementary mechanical load.

$$K = \frac{1}{\max\left(\frac{\varepsilon_{oi}}{\varepsilon_{mi}}\right)} = \min\left(\frac{\varepsilon_{mi}}{\varepsilon_{oi}}\right) \tag{41}$$

This relation is correct in the case where, after each basic load, the induced strain returns to a zero value (Fig. 63).

But in the case of mechanical load increments (Fig. 64) this relation is not applicable. In this case, the damage could be expressed by:

$$\mathcal{D} = \sum_{i=1}^{N} \frac{\Delta\varepsilon_{oi}}{\varepsilon_{mi}} \tag{42}$$

$\Delta\varepsilon_{oi}$ = Equivalent strain increment resulting from mechanical load $i$;
$\varepsilon_{mi}$ = strain capability at mechanical load $i$.

Therefore, the factor of safety is written as:

$$K = \frac{1}{\sum_{i=1}^{N} \frac{\Delta\varepsilon_{oi}}{\varepsilon_{mi}}}$$

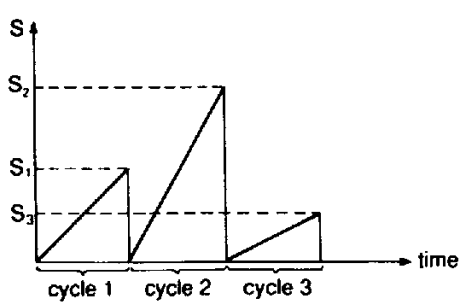


FIG. 6.63. Cumulation of mechanical loading.



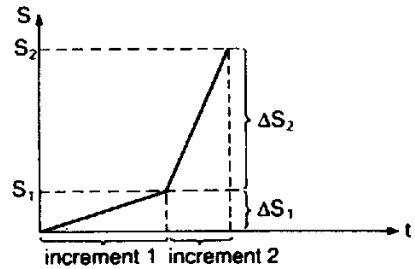


FIG. 6.64. Loading increments.

The calculation of the factor of safety based on the strains presents a very distinct advantage for case-bonded grains. In these grains the two important mechanical loads are due to temperature changes and pressure rise at firing. For these mechanical loads the strains are not dependent on the behavior of the propellant when it is used in its incompressible portion.

That is why research continues, so that a relation can be determined which takes the cumulation of strains into consideration, specifically in the case of tensile stress with simultaneous temperature changes [34].

### 6.1.3. *Factor of safety defined with stresses*

For an elementary mechanical load, this is defined by:

$$K_\sigma = \frac{\sigma_m}{\sigma_o}$$

where:

$\sigma_m$ = maximum stress for the loading rate and temperature parameters corresponding to the applied mechanical load;
$\sigma_o$ = equivalent stress at the most stressed point, assessed through calculations using the failure criterion.

The cumulation of induced stresses presents the same problem, whether the basic factors of safety were determined from the stresses or the strains.

It is possible, however, to establish empirical rules based on observations made in the course of simple tests, provided that these rules constantly remain subject to revision.

The following rule can be proposed

$$K_\sigma = \frac{\sigma_o(t)}{\sigma_m(t)}$$

where:

$\sigma_o(t)$ = stress cumulation existing in the propellant grain at time $t$;
$\sigma_m(t)$ = stress capability of the propellant under the total load conditions at time $t$.

Unfortunately, with a case-bonded grain, the induced stresses are often dependent on the behavior of the propellant; consequently, to obtain a reliable factor of safety, it is important to know that behavior.

## 6.2. BONDING FACTOR OF SAFETY

The assessment of the safety factor of the bonding is always done using stress. Several failure criteria can be used for bondings:

- normal stress criterion;
- shear stress;
- surfacic force applied at the bondline ($\sigma_N$, $\tau$).

In every case the factor of safety is defined by the ratio between the capability (obtained experimentally as described in Section 4.3.3) and the induced stress using one or the other failure criteria.

The failure criterion expressed in force seems to be best suited.

In every case the factor of safety in relation to the propellant is calculated at the critical point of the bonding. When it is found to be smaller than one of the factors of safety obtained from the bonding failure criteria, it is used to characterize the bonding.

In the case of the induced stress resulting from firing, the importance of the effect of the pressure varies, based on whether the grain has been stress-relieved (prepared debonding), or completely bonded. For a stress-relieved grain the most stressed point of the bonding is located fairly far from the burning surface. Should debonding occur during pressure rise, the propellant is pressed again against the liner and the risk of propagation is rather low. In addition, since the flame reaches the debonding at the end of the firing, the operation of the motor is not affected.

But in the case of an entirely bound grain, the critical point is located very close to the free surface, i.e. the combustion chamber. A debonding in that area has a high level of probability of opening into the combustion chamber creating at the time of firing an additional burning surface, and therefore a faulty operation of the motor (Fig. 65). In this case the effect of the pressure on the normal stress must be taken into account.

*Comment.* As with propellant (Section 6.1.1.) there is the problem of damage cumulation for the propellant-liner bonds. Research is being done in that area [28]. The cumulative damage laws described in Section 6.1.1 can, however, be used for the propellant-liner bonds, even though the bond failures always occur in the propellant.



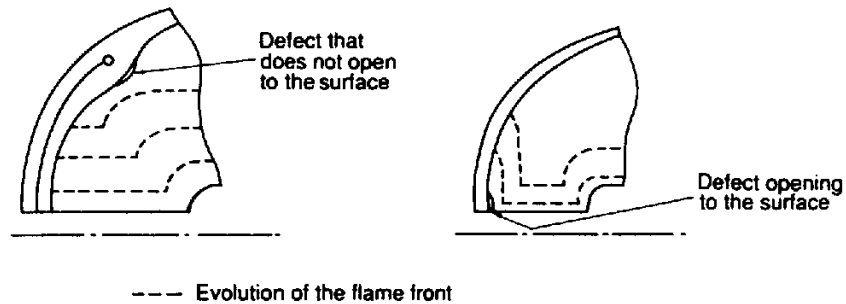


FIG. 6.65.

## 6.3. VERIFICATION AND ADJUSTMENT OF VARIOUS METHODS OF ANALYSIS OF FACTORS OF SAFETY

Verification of the methods cannot be done on a large number of propellant grains when these are either expensive or of large size.

It is therefore desirable to design objects that are small in size, inexpensive, simple to use, and allow the creation in the propellant of induced stresses/strains identical to those occurring in propellant grains. Several objects, of varying geometry, have been proposed, including the SEC model developed in the United States [29], and the PHI model from France [30] (Figs 66 and 67).

These objects are subjected to various thermal cycles or to pressurizations until the propellant fails. These are used to evaluate the various methods used to calculate the factor of safety in the case of cumulative mechanical stresses.

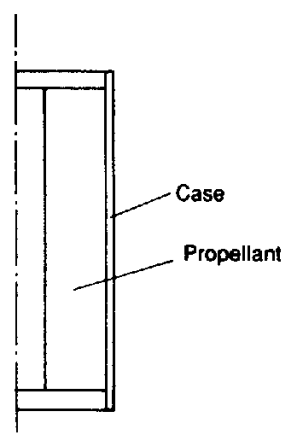


FIG. 6.66. S.E.C. model.

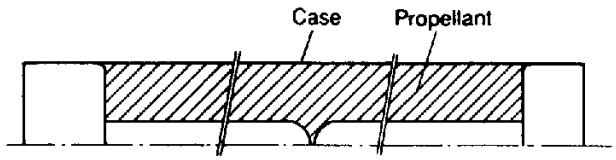


FIG. 6.67. PHI model.

The PHI model offers the distinct advantage of very different induced load levels simply by modifying several geometrical parameters (Fig. 68):

- inside diameter;
- diameter of the hole in the membrane;
- thickness of the membrane;
- length of the model.

In addition, as it is the case for many propellant grains, the location of the most stressed point in the PHI model is clearly known, and the volume of propellant heavily stressed around that point is small in comparison with the total volume of the propellant. On the other hand, in the SEC model, the volume of propellant heavily stressed is much larger.

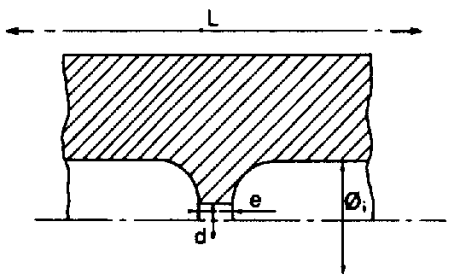


| | | Ø_i = 20 | 24 | 30 | |
|---|---|---|---|---|---|
| e = 5 mm | d = 4 mm | 9,7% | | | L = 1000 mm |
| | d = 8 mm | | | 4,8% | |
| e = 10 mm | d = 4 mm | 8,8% | | | |
| e = 5 mm | d = 4 mm | 7,8% | 6,5% | 4,8% | L = 600 mm |

$\alpha = 1{,}2 \quad 10^{-4}\,°C^{-1} \qquad \Delta T = 10°C$

FIG. 6.68. Maximum strain as a function of the geometry of the PHI model.



### 6.4. SEMI-EXPERIMENTAL DETERMINATION OF THE FACTOR OF SAFETY

When dealing with propellant grains with a complex geometry, subjected to induced stresses/strains for which it is difficult to develop models (thermal cycles, for example), semi-experimental methods can be used to calculate the factor of safety.

*Phase 1.* A finite element analysis is done on the three-dimensional geometry with an incompressible linear elastic behavior, for a simple mechanical load (uniform temperature change, for example), and the strain field is determined.

*Phase 2.* A PHI model is selected (Fig. 67). Its geometrical dimensions are such that they allow the same strain level under the same analysis conditions: same behavior law, same boundary conditions.

*Phase 3.* The PHI model is made with the propellant that needs to be tested. It is subjected to the same cycles as the propellant grains being analyzed.

If the specimen breaks during the cycling, the factor of safety propellant grain is lower than 1. It will therefore be necessary to modify either the propellant or the geometry of the grain.

If the specimen does not fail, it is subjected to a $N$ number of cycles, identical to the preceding one, until failure occurs.

If the propellant obeys a damage law of the form (24), one can write, for a cycle:

$$D = \left(\frac{1}{N}\right)^{1/m}$$

and

$$K = N^{1/m}$$

This allows us to determine the order of magnitude of the factor of safety.

The steps involved in this method are shown in Fig. 69.

## 7. Propellant Behavior Under Dynamic Loads

### 7.1. LOW AMPLITUDES

Propellant grains are subjected to this type of load during transport or during a defective operation of the rocket motor (combustion instabilities, for example). The loads, in these conditions, can be written in terms of Fourier

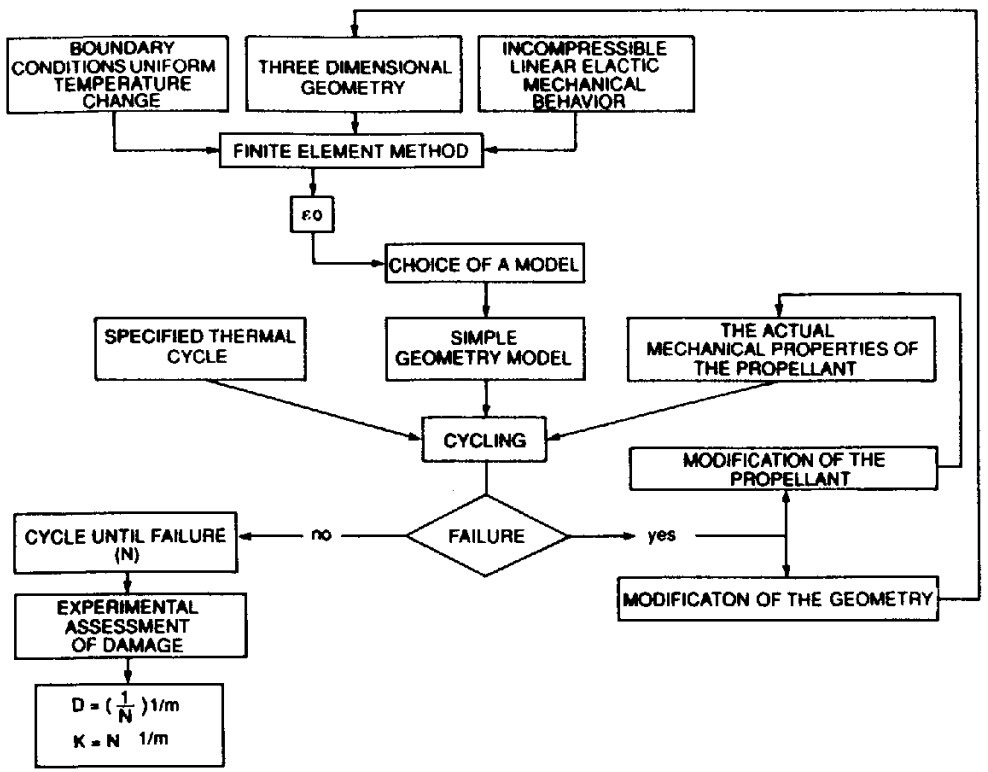


FIG. 6.69. Semi-experimental determination of the factor of safety.

series, and the propellant behavior is determined as a function of the frequency. Two methods are used:

- viscoanalyzer (1-1,000 Hz);
- ultrasounds (0.5-2.5 MHz).

The expression of the modulus of a propellant under harmonic stress loading takes the form of a complex number.

$$E^* = E' + iE''$$

$$tg\delta = \frac{E''}{E'}$$ expresses the damping of the material.

Figures 70.1 and 70.2 illustrate the aspect of the master curve of the dynamic modulus with which the time-temperature equivalence principle can be applied.



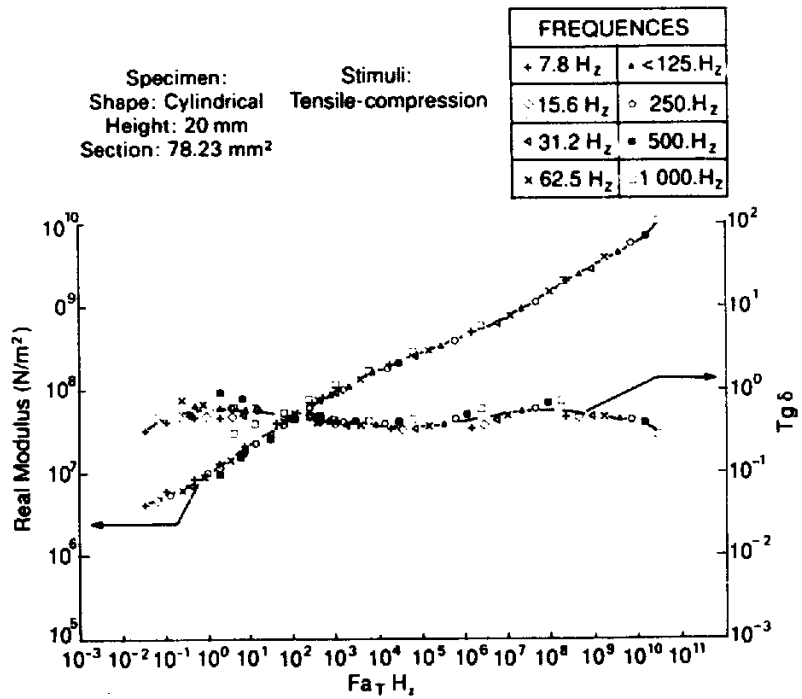


FIG. 6.70(1). Dynamic tests. Viscoelasticimeter.

## 7.2. HIGH AMPLITUDES

The propellant grains may be subjected to rapidly varying loads, usually considered as shocks. These are loads that could have a dynamic impact, very high amplitudes, rendering Fourier series analyses useless because behavior non-linearity occurs. These loads may cause a fragmentation of the propellant. When these fragments are smaller than a critical size, a transition phase may occur in the combustion regime for some propellants, leading to a mass detonation of the rocket motor.

These studies are all concerned with the safety of the motors; they are discussed in Chapter 7. The experimental methods that help characterize the propellant behavior are as follows:

- rapid tensile loading machine with a displacement rate of 20 m/s;
- Hopkinson bars;
- impact against flat wall;
- shock Hugoniot measurements with a light gas gun.

The study of the impact behavior on a propellant is discussed in many research papers ([31-33], among many others), and could fill an entire

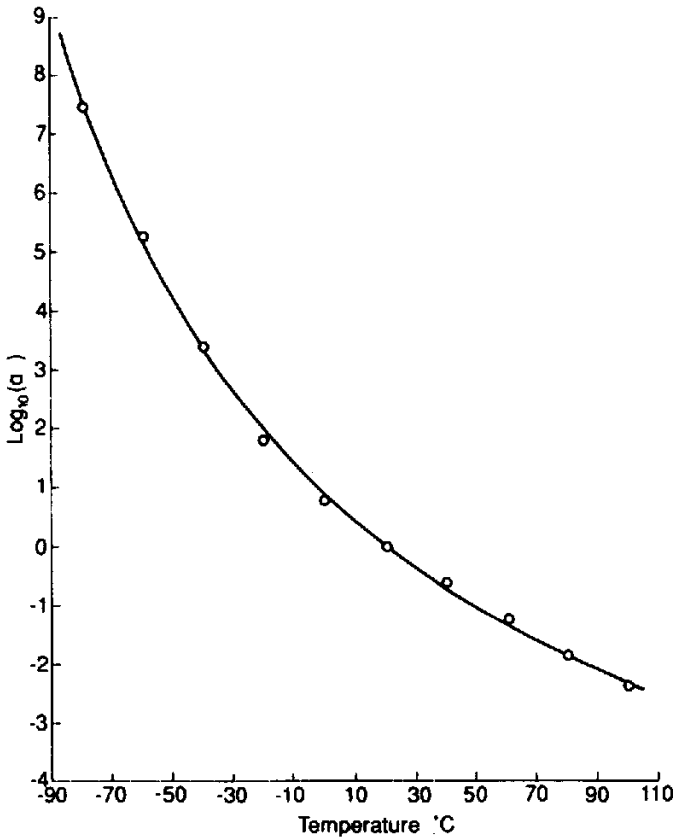


FIG. 6.70(2). Time-temperature equivalence factor.

chapter. A detailed description of the result of these studies cannot be given here. It is important, however, to indicate that in the case of composite propellants, the behavior of the crystalline oxidizers has a major effect on the behavior of the propellant, while in the case of static loads, whose rates are much lower, the propellant behavior is mostly dependent on the bonding between the binder and the crystalline oxidizer.

## 8. Conclusions and Future Prospects

With a method which would allow a precise determination of the factor of safety of a propellant grain it would be possible to optimize the performance of rocket motors through a potential increase in the volumetric loading fraction of the grain.



The methods used nowadays are still somewhat imprecise in some cases, and need to be improved. They have, however, made it possible to improve propellant grain designs. Even though there is no perfect model of the propellant behavior, the research work has helped us obtain a better understanding of the phenomena and, indirectly, assisted in the formulation of new compositions.

A high level of activity must be continued in this area to model the behavior of propellants and their fracture mechanisms. At the same time, numerical analysis techniques must evolve further to take the actual propellant behavior into account, at the lowest possible cost.

Finally, all of the research must be based on many experimental results obtained from tests performed on propellant grains or models.

## Bibliography

1. PERSOZ, B., *Introduction à l'étude de la rhéologie*. Dunod.
2. CHRISTENSEN, R. M., *Theory of Viscoelasticity: An Introduction*. Academic Press.
3. FERRY, J. D., *Viscoelastic Properties of Polymers*. Ed. J. Villey, 1970.
4. FARRIS, R. J., Development of Solid Rocket Propellant Non-Linear Viscoelastic Constitutive Theory. AFRPL-Tr-75-20, May 1975.
5. PARASKEVAS, Etude théorique et expérimentale de la photoélasticimétrie tridimensionnelle. Rapport CETIM No. 15 G 151.
6. ZIENKIEWICZ, O. C., *La méthode des éléments finis* (traduit de la 3ème édition anglaise). McGraw-Hill.
7. TOUZOT, G., Une présentation de la méthode des éléments finis. Presse de l'Université Laval (Quebec).
8. MARTIN, Ch., RACIMOR, P., LE ROY, M. and QUIDOT, M., Représentation par des lois de Farris du comportement viscoélastique non linéaire d'un matériau chargé. Groupe Français de Rhéologie. December 1980.
9. MELI, G., THEPENIER, J., PASQUIER, M. and DUBROCA, G., Mechanical design of case bonded CMDB grains by a non linear viscoelastic method. AIAA, SAE, and ASME Joint Propulsion Conference, Vol. 16, No. 80-1177, 1980.
10. WILLIAMS, M. L., LANDEL, R. F. and FERRY, J. D., The temperature dependence of relaxation mechanisms in amorphous polymers and other glass-forming liquids. *J. Am. Chem. Soc.*, 77(3), 701, 1955.
11. BOLEY, B. A. and WEINER, J. H., *Theory of Thermal Stresses*. 1st edition. John Wiley, New York. 1960.
12. REISMANN, H. and PAWLIK, P. S., *Elasticity Theory and Applications*. John Wiley and Sons.
13. FRANCIS, E. C. *et al.*, Propellant Non-Linear Constitutive Theory Extension: Preliminary Results. UTC/CSD-2742-AFRPL-TR-83-034, August 1983.
14. TSCHOEGL, N. W., *Failure Surfaces in Principal Stress Space*. Polymer Science Symposium No. 32, 239-267. John Wiley and Sons. 1971.
15. LANGLOIS, G. and GONARD, R., New law for crack propagation in solid propellant material. *J. Spacecraft Rockets*, 16, 357, 1979.
16. NOTTIN, J. P., GONDOUIN, B. and LUCAS, M., Experimental investigation of cracks growth in composite propellants. AIAA 85-1437. AIAA/SAE/ASME/ASEE 21st Joint Propulsion Conference. Monterey, California, 1985.
17. SCHAPERY, R. A. *Int. J. Fracture*, 11, 141, 1975; *International Journal of Fracture*, 11, 369, 1975; *Int. J. Fracture*, 11, 549, 1975.
18. KNAUS, W. G., On steady propagation of a crack in a viscoelastic sheet: experiments and analysis. *Deformation and Fracture of High Polymers*, edited by J. Henning Kausch, Hohn A. Hassel and Robert K. Jaffee. Plenum Press, 1974.

19. BECKWITH, S. W. and WANG, D. T., *Crack Propagation in Double-Base Propellants.* Hercules Incorporated Bacchus Works, Magna, Utah.
20. HERRMANN, L. R., Elasticity equations for incompressible and nearly incompressible materials by a variational theorem. *AIAA Journal*, 3, 1886-1900, 1965.
21. SHAPERY, R. A., *A Micromechanics Model for Non-Linear Viscoelastic Behavior of Particle-Reinforced Rubber with Distributed Damage.* Texas A & M University, College Station, Texas. MM 4867-86-1, January 1986.
22. GREEN, A. E., and ZERNA, W., *Theoretical Elasticity.* Clarendon Press, Oxford, 1968.
23. WANG, D. T., and SHEARLY, R. N., A review of solid propellant grain structural margin and safety prediction methods. AIAA/ASME/SAE/ASEE 22nd Joint Propulsion Conference. AIAA Paper No. 86-1415, 1986.
24. BILLS, K. W., Jr., *et al.*, Non-linear fracture mechanics. Final Report. NWC-TP-5684. February 1975.
25. MINER, M. A., Cumulative damage in fatigue. *J. Appl. Mech., Trans. ASME, Series E*, 67, 1945.
26. LIU, C. T., Crack growth behavior in composite propellant with strain gradient. AIAA/ASME/SAE 20th Joint Propulsion Conference, June 1984.
27. PARR, C. H., End effect due to shrinkage in solid propellant grains. *Bulletin of the 20th JANAF Panel on Physical Properties of Solid Propellants*, Vol. 1, November 1961.
28. BILLS, K. W., Jr *et al.*, A cumulative damage concept for propellant-liner bonds in solid rocket motors. *J. Spacecraft*, 3, 3, 1966.
29. ICRPG, *Solid Propellant Mechanical Behavior Manual*, CPIA Publications, 1963.
30. THEPENIER, J., GONDOUIN, B., and MENEZ-COUTENCEAU, H., Reliability of solid propellant grains: mechanical analog motor design and testing. AIAA/SAE/ASME/ASEE 23rd Joint Propulsion Conference, AIAA-87, 1987.
31. STANKIEWICZ, F., HUMBERT, P. and BOULE, P., Effect of dynamic loading on fracture behavior of filled polymers. *Impact Loading and Dynamic Behavior of Materials.* DGM Information Gesellschaft Verlag, Vol. 1, 1988.
32. QUIDOT, M., Dynamic fragmentation of compact energetic materials. *Impact Loading and Dynamic Behavior of Materials.* DGM Information Gesellschaft Verlag, Vol. 2, 1988.
33. Mechanical Properties at High Rates of Strain, Conference, Oxford, edited by J. Harding, March 1979.
34. RACIMOR, P. and NOTTIN, J. P., Mechanical behavior of solid propellants during tensile test with variable temperature. AIAA/ASME/SAE/ASEE, 25th Joint Propulsion Conference No. 89-2645.